J Opt
https://doi.org/10.1007/s12596-024-01931-w

RESEARCH ARTICLE

Chalcone derivatives with strong nonlinear optical activity

Djebar Hadji[1,2] · Toufik Bensafi[2] · Benamar Baroudi[3]

Received: 22 March 2024 / Accepted: 26 May 2024

Abstract In this quantum chemical investigation, first-principles calculations based on density functional theory are successfully employed to calculate and analyse in detail the electrical properties (dipole moment, polarizability, and first hyperpolarizabilities) of seven chalcone-based derivatives using five DFT functionals (B3LYP, PBE0, ωB97X-D, CAM-B3LYP, and M06-2X). The variations of (hyper)polarizability as a function of the chalcone structures are consistent among the different levels, facilitating the deduction of structure–property relationships. The properties have been calculated and extensively analyzed to highlight nonlinear optical activity. The obtained results show a high total first hyperpolarizability β_{tot} up to 5766 a.u. and low energy gap E_g less than 2.15 eV. An inverse relationship has been obtained between the β_{tot} and E_g. This quantum chemical exploration of chalcones with high hyperpolarizabilities will provide more insights into exploring novel nonlinear optical materials and progressing in technologies that rely on manipulating and controlling light for various purposes, such as optical signal processing, photonic devices, and photorefractive devices.

Supplementary Information The online version contains supplementary material available at https://doi.org/10.1007/s12596-024-01931-w.

✉ Djebar Hadji
hadji120780@yahoo.fr; djaber.hadji@univ-saida.dz

[1] Department of Chemistry, Faculty of Sciences, University of Saida – Dr. Moulay Tahar, 20000 Sidon, Algeria

[2] Modeling and Calculation Methods Laboratory, University of Saida – Dr. Moulay Tahar, 20000 Sidon, Algeria

[3] Department of Chemistry, Faculty of Exact Sciences and Computer Science, University of Hassiba Benbouali, 02000 Chlef, Algeria

Graphical abstract

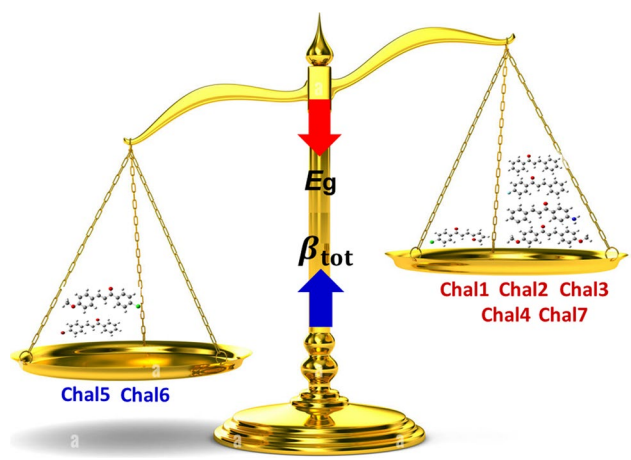

Keywords Chalcone · Chlorine · Furane · Methoxy · Nonlinear optics

Introduction

Over the recent few decades, organic aromatic delocalized π-electron systems and other analogue fragments combined with strong electron donating and strong electron-withdrawing groups have become one of the largest classes of organic materials. It has been the subject of significant interest to several researchers worldwide in recent decades, where about 50% of all chemical compounds synthesized by the end of the second millennium are aromatic derivatives. The first synthesis of chalcone by Claisen and Claparede [1] was prepared by aldol condensation reactions between aromatic aldehydes and acetophenones using sodium methoxide as a

Published online: 17 June 2024

condensing agent. In recent years, much attention has been given to organic compounds containing chalcone scaffolds due to their interesting structure, which is the main essential constituent of many natural or synthetic sources. Chemically, the chalcone derivatives as another's electronically rich system have two aromatic rings that are joined by a three-carbon α, β-unsaturated C=O group of plant-derived polyphenolic compounds belonging to the flavonoids and isoflavonoids family [2, 3]. Moreover, the chalcone parent ring with raw formula $C_6H_5C(O)CH{=}CHC_6H_5$, therefore, exists in two stereoisomers (Z and E) depending on the arrangement of substituents around the central double bond with planar conformation structure. In chalcones (Chals), the π-electrons are delocalized and are easily polarizable. Chals and their other associated derivatives allow good work, so a range of new aromatic with good optical materials [4]. Chals class molecules play an essential role in chemical reactions [5]. Chalcone scaffold represents a common motif in many pharmaceutical active and remarkable compounds demonstrating a wide range of pharmacological activities; the essential activities are antioxidant [6], antifungal [7], antimicrobial [8], and anti-inflammatory [9], in addition, the chalcone fragment and their privileged analogues are a class of compounds with cross conjugated (nonlinear optical) NLO chromophores that are reported to exhibit with efficient blue and yellow light transmittance [10], good crystallizability [11], transparency [12], and large second harmonic generation SHG efficiency [11]. Chemical properties with π-conjugated chalcone and its derivatives are of interest due to their wide excellent applications in fields such as molecular switching, frequency doubling, and optical limiting [13]. The molecular structure of organic compounds greatly influences their optoelectronic properties by affecting conjugation length, the presence of functional groups, molecular packing, and resonance effects. The comprehension and regulation [14, 15] of these structural parameters are essential for optimizing the performance of organic optoelectronic devices [16]. The degree of π-conjugation along the molecular backbone significantly impacts the optoelectronic properties [17]. Longer conjugation lengths allow for greater delocalization of π-electrons, resulting in narrower band gaps and enhanced absorption of light across a wider range of wavelengths. Moreover, the presence of functional groups in those materials can alter their optoelectronic properties [18, 19] by modifying the energy levels of molecular orbital and introducing additional electronic transitions. Electron-donating or electron-withdrawing functional groups can shift the energy levels of the HOMO and LUMO, thereby affecting the band gap and absorption/emission spectra of the material [18, 19]. Structural engineering of materials serves as a cornerstone for advancing the field of NLO optics, driving innovation in optical materials design, device technology, and photonic applications [20, 21]. By harnessing the power of molecular and crystal engineering, researchers can unlock the full potential of NLO materials for next-generation optical technologies. Altering the molecular architecture through strategies such as incorporating electron-donating and electron-withdrawing groups [22] into the molecular structure creates a push–pull architecture. Also, the introduction of functional groups [18] that promote favourable intermolecular interactions, enhance solubility, or improve film-forming properties can optimize the performance of NLO materials, additionally, combining different types of NLO-active components, such as metals [23], complexes [20], organic molecules, or polymers, can lead to synergistic effects and tailored NLO responses. By applying these strategies, researchers can tailor the structural properties to achieve enhanced NLO optical responses. Various electron-withdrawing groups, including F, Cl, Br, I, CF_3, and CN, have been included at the end and lateral terminal positions of terpyridine-substituted hexamolybdates to build different molecular systems [19]. The β values are considerably influenced by the addition of halogens at the terminus of the terpyridine ligand, as it establishes a robust D–bridge–A structure. Conversely, the presence of CF_3 and CN substantially impacts the second-order molecular reaction. Similarly, Janjua et al. [24] have documented the occurrence of additional POM-clusters connected to terpyridine units by bridging groups. In addition, the research [25] employs machine-learning techniques to evaluate the suitability of small-molecule donors for organic solar cells. Moreover, an alternative methodology [26] has been employed to address the development of novel dye designs through the structural modification of π-spacers/conjugated systems and terminal acceptors. The computational studies of NLO properties of materials based on chalcone derivatives have been studied at various DFT levels and compared with the experimental results [4]. From the literature, it has been found that among the reported NLO chalcone derivatives, only a few Chals have been investigated both experimentally and theoretically due to their potential applications in photonics and optoelectronics [27, 28]. In the present work, we focused on the theoretical analysis of linear and NLO properties of seven chalcones (Chal1–Chal7) [29] (Scheme 1) using density functional theory (DFT) at five levels of theory. The methods based on DFT represent an important road since they allow the simulation of a wide range of molecular properties with high precision. Recently, DFT calculations have successfully been used to evaluate the NLO properties of chalcone derivatives [30, 31] to contribute to this series of investigations, in the present study, we investigate the impact of various substituted donor/acceptor strength on the dipole moment, polarizability, first hyperpolarizability, and energy gap E_g. This new study will focus on the relation between the higher hyper-Rayleigh scattering (HRS) hyperpolarizability β_{HRS} and the electric field-induced second harmonic

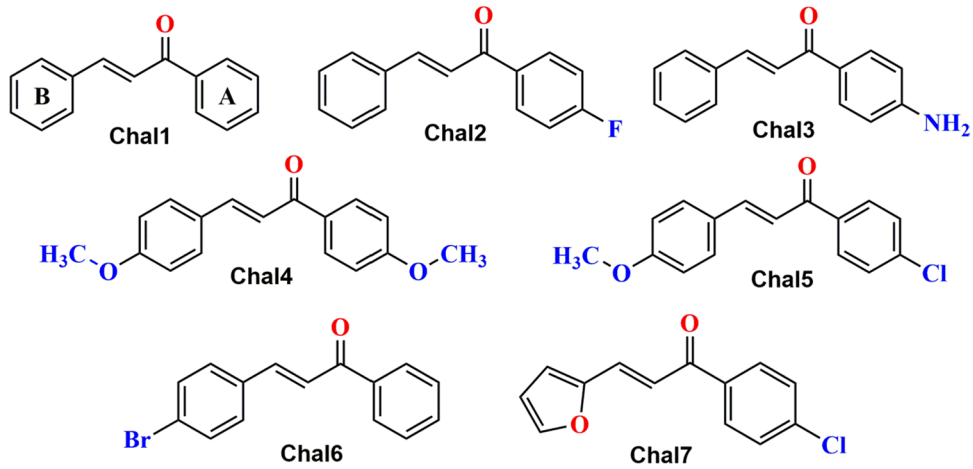

Scheme 1 Structure of seven chalcone-based molecules Chal1–Chal7

generation (EFISHG) $\beta_{//}$, and the relation between the first hyperpolarizability β and the energy gaps of these Chals. While these properties are related to the electronic structure of Chals, they are not directly proportional to each other. However, they can be influenced by similar factors such as molecular size, shape, symmetry, and electronic configuration. There might be correlations between these properties in certain cases, but they are not simple proportional relationships. We also investigated the frontier molecular orbitals (FMOs) HOMO and LUMO, their energies, the location, and the nature of the isosurfaces. The FMOs analysis has been used to elucidate information regarding the ionization potential (I), electron affinity (A), global hardness (η), global softness (S), chemical potential (V), electronegativity (χ), and global electrophilicity index, (ω), nucleophilicity index (N). The examined Chals demonstrate attractive NLO characteristics that can be utilised for practical purposes in many domains. The present study is anticipated to yield valuable insights for researchers in the field of optoelectronics, specifically in the areas of greenhouse-integrated solar cells [32] and hole transport materials [33, 34]. These materials have the potential to enhance the power conversion efficiency and stability of organic solar cells [35].

Methodologies

All theoretical computations were performed with density functional theory at the 6-311++G** basis set implemented in Gaussian 09 [36]. The optimized structures and their coordinates are performed using the B3LYP/6-311++G** level and presented in Fig. 1 and Tables S1-S7 in supporting information SI, respectively. The B3LYP balanced treatment of exchange and correlation effects allows for accurate predictions of molecular geometries, vibrational frequencies, and electronic properties [37, 38]. Additionally, the B3LYP has been found to perform well for organic compared to many modern-day XC functionals [37, 38]. The visualization of the Chal1, Chal2, Chal3, Chal4, Chal5, Chal6, and Chal7 optimized geometries, HOMO, and LUMO plots has been carried out using GaussView 5.1 [39]. Linear (dipole moment μ, mean polarizability $\langle\alpha\rangle$, polarizability anisotropy $\Delta\alpha$) and NLO properties (total first hyperpolarizability β_{tot}, electric-field-induced second harmonic generation (EFISHG) $\beta_{//}$, hyper-Rayleigh scattering (HRS) first hyperpolarizability β_{HRS}, and the depolarization ratio DR) were calculated at the B3LYP [40, 41], PBE0 [42], CAM-B3LYP [43], ωB97X–D [44], and M06–2X [45] methods using the 6-311+G** basis set. The scattering intensity $I^{2\omega}_{\Psi V}$ corresponding to the polarization angle Ψ was obtained by the Multiwfn 3.7 [46]. Studies show the suitability of the corrected XC functionals to calculate α and β [47, 48].

μ is defined as:

$$\mu = \sqrt{\left(\mu_x^2 + \mu_y^2 + \mu_z^2\right)} \tag{1}$$

$\langle\alpha\rangle$ was calculated from as [49]:

$$\langle\alpha\rangle = \frac{1}{3}\sum_{i=x,y,z}\alpha_{ii} \tag{2}$$

$$\langle\alpha\rangle = \frac{1}{3}\left(\alpha_{xx} + \alpha_{yy} + \alpha_{zz}\right) \tag{3}$$

and the $\Delta\alpha$ as:

$$\Delta\alpha = \sqrt{\frac{1}{2}\left(\left(\alpha_{xx} - \alpha_{yy}\right)^2 + \left(\alpha_{xx} - \alpha_{zz}\right)^2 + \left(\alpha_{yy} - \alpha_{zz}\right)^2\right)} \tag{4}$$

For β, we are interested in $\beta_{//}$ and β_{HRS}. The $\beta_{//}$ is the central quantity of β vector projected along the μ-axis and calculated as:

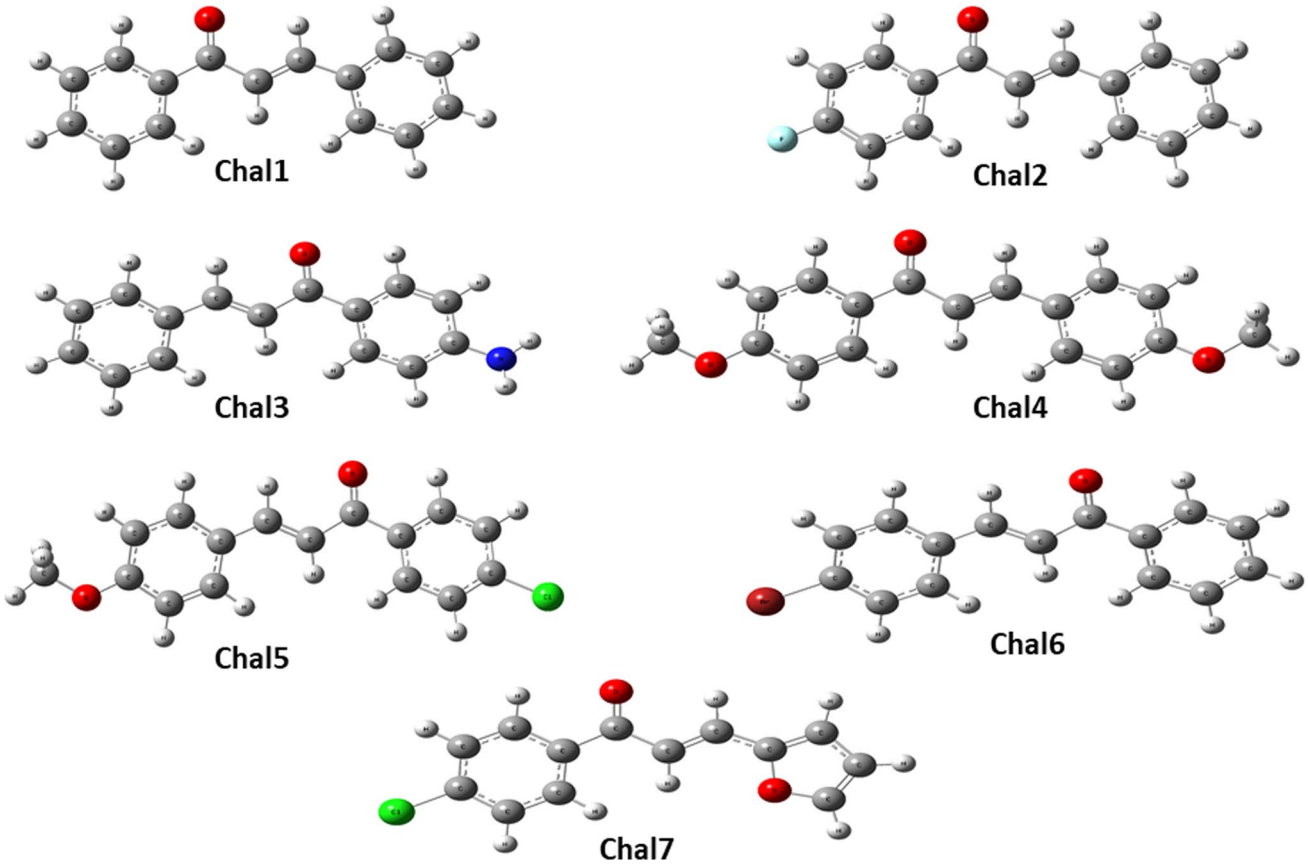

Fig. 1 Chal1–Chal7 optimized structure at the B3LYP/6-311+G** level

$$\beta_{//}(-2\omega,\omega,\omega) = \beta_{//} = \frac{1}{5}\sum_{\mathrm{i}}\frac{\mu_{\mathrm{i}}}{|\vec{\mu}|}\sum_{\mathrm{j}}\left(\beta_{ijj}+\beta_{jij}+\beta_{jji}\right) \quad (5)$$

In the static limits ($\beta_{\mathrm{ijj}} = \beta_{\mathrm{jij}} = \beta_{\mathrm{jji}}$), $\beta_{//}$ becomes

$$\beta_{//} = \frac{3}{5}\sum_{i=x,y,z}\frac{\mu_{\mathrm{i}}\beta_{\mathrm{i}}}{|\vec{\mu}|} \quad (6)$$

$|\vec{\mu}|$ is the norm of the dipole moment, μ_{i} and β_{i} the ith components of μ and β vectors, respectively. The β_{HRS} is related to the $I^{2\omega}_{\Psi V}$ for nonpolarized incident light of frequency ω, and observation of plane-polarized scattered light made perpendicular to the propagation plane. The β_{HRS} is calculated as

$$\beta_{\mathrm{HRS}} = \langle\beta^2_{\mathrm{HRS}}\rangle = \langle\beta^2_{\mathrm{ZZZ}}\rangle + \langle\beta^2_{\mathrm{ZXX}}\rangle \quad (7)$$

$$DR = \frac{I^{2\omega}_{\mathrm{VV}}}{I^{2\omega}_{\mathrm{HV}}} = \frac{\langle\beta^2_{\mathrm{ZZZ}}\rangle}{\langle\beta^2_{\mathrm{ZXX}}\rangle} \quad (8)$$

$\langle\beta^2_{\mathrm{ZZZ}}\rangle$ and $\langle\beta^2_{\mathrm{ZXX}}\rangle$ given by the molecular (x, y, z) reference are averages of β components that describe the isotropic distribution of molecular orientations in dilute solutions. $\langle\beta^2_{\mathrm{ZZZ}}\rangle$ and $\langle\beta^2_{\mathrm{ZXX}}\rangle$ were calculated without assuming Kleinman's conditions, and the temperature convention was used for defining the β quantities. The detailed expressions of $\langle\beta^2_{\mathrm{ZZZ}}\rangle$ and $\langle\beta^2_{\mathrm{XZZ}}\rangle$ [50] are shown in the SI.

$$\begin{aligned}\langle\beta^2_{\mathrm{ZZZ}}\rangle = {} & \frac{1}{7}\sum\nolimits_{\zeta}^{x,y,z}\beta^2_{\zeta\zeta\zeta} + \frac{4}{35}\sum\nolimits_{\zeta\neq\eta}^{x,y,z}\beta^2_{\zeta\zeta\eta} \\ & + \frac{2}{35}\sum\nolimits_{\zeta\neq\eta}^{x,y,z}\beta_{\zeta\zeta\zeta}\beta_{\zeta\eta\eta} + \frac{4}{35}\sum\nolimits_{\zeta\neq\eta}^{x,y,z}\beta_{\eta\zeta\zeta}\beta_{\zeta\zeta\eta} \\ & + \frac{4}{35}\sum\nolimits_{\zeta\neq\eta}^{x,y,z}\beta_{\zeta\zeta\zeta}\beta_{\eta\eta\zeta} + \frac{1}{35}\sum\nolimits_{\zeta\neq\eta}^{x,y,z}\beta^2_{\eta\zeta\zeta} \\ & + \frac{4}{105}\sum\nolimits_{\zeta\neq\eta\neq\varepsilon}^{x,y,z}\beta_{\zeta\zeta\eta}\beta_{\eta\varepsilon\varepsilon} + \frac{1}{105}\sum\nolimits_{\zeta\neq\eta\neq\varepsilon}^{x,y,z}\beta_{\eta\zeta\zeta}\beta_{\eta\varepsilon\varepsilon} \\ & + \frac{4}{105}\sum\nolimits_{\zeta\neq\eta\neq\varepsilon}^{\mathrm{x,y,z}}\beta_{\zeta\zeta\eta}\beta_{\varepsilon\varepsilon\eta} + \frac{2}{105}\sum\nolimits_{\zeta\neq\eta\neq\varepsilon}^{\mathrm{x,y,z}}\beta^2_{\zeta\eta\varepsilon} \\ & + \frac{4}{105}\sum\nolimits_{\zeta\neq\eta\neq\varepsilon}^{\mathrm{x,y,z}}\beta_{\zeta\eta\varepsilon}\beta_{\eta\zeta\varepsilon}\end{aligned} \quad (9)$$

$$\langle \beta_{XZZ}^2 \rangle = \frac{1}{35}\sum_{\zeta}^{x,y,z}\beta_{\zeta\zeta\zeta}^2 + \frac{4}{105}\sum_{\zeta\neq\eta}^{x,y,z}\beta_{\zeta\zeta\zeta}\beta_{\zeta\eta\eta} - \frac{2}{35}\sum_{\zeta\neq\eta}^{x,y,z}\beta_{\zeta\zeta\zeta}\beta_{\eta\eta\zeta} + \frac{8}{105}\sum_{\zeta\neq\eta}^{x,y,z}\beta_{\zeta\zeta\eta}^2 + \frac{3}{35}\sum_{\zeta\neq\eta}^{x,y,z}\beta_{\zeta\eta\eta}^2 - \frac{2}{35}\sum_{\zeta\neq\eta}^{x,y,z}\beta_{\zeta\zeta\eta}\beta_{\eta\zeta\zeta} + \frac{1}{35}\sum_{\zeta\neq\eta}^{x,y,z}\beta_{\zeta\eta\eta}\beta_{\zeta\varepsilon\varepsilon} - \frac{2}{105}\sum_{\zeta\neq\eta\neq\varepsilon}^{x,y,z}\beta_{\zeta\zeta\eta}\beta_{\eta\varepsilon\varepsilon} + \frac{2}{35}\sum_{\zeta\neq\eta\neq\varepsilon}^{x,y,z}\beta_{\zeta\eta\varepsilon}^2 - \frac{2}{105}\sum_{\zeta\neq\eta\neq\varepsilon}^{x,y,z}\beta_{\zeta\eta\varepsilon}\beta_{\eta\zeta\varepsilon} \quad (10)$$

Results and discussion

Linear and NLO results

Dipole moment

Generally, the double bond between the α and β carbon C atoms of the carbonyl group C=O influenced the μ in Chal molecules. μ arises due to the difference in electronegativity between the atoms involved in the bond. The C=O group consists of a carbon–oxygen double bond, where O is more electronegative than C. The O atom pulls the electron density towards itself, creating a μ with a partial negative charge on the O and a partial positive charge on the C. The presence of substituents in the Chal can also affect the overall μ. In this exploration, we study seven Chals where the substituent has a significant electronic effect that modulates some overall molecular properties (μ, α, and β), which were corroborated by combining theoretical results. The most fundamental property of the electrical responses is μ. Therefore, determining these values has given rise to a solid foundation for discussing the calculation accuracy of the different theoretical methods. The different μ values of seven Chals obtained using the B3LYP, PBE0, CAM-B3LYP, ωB97X–D, and M06–2X levels at the 6-311+G** basis set are displayed in Table 1. In Fig. 2, we showed the μ vector of our studied Chals. An accurate analysis of these results shows that the B3LYP and PBE0 functionals give the highest μ values, while the M06-2X functionals give the lowest μ values. The CAM-B3LYP and ωB97X–D levels show systematically smaller μ values. The calculated μ values vary between 1.60 and 5.38 D. The variation of μ as a function of DFT functionals attain a maximum of ~5% for Chal1, ~6% for Chal2, ~7% for Chal3, ~22% for Chal4, ~9% for Chal5, ~4% for Chal6, and ~5% for Chal7 (Table 1 and Fig. 3). The B3LYP and PBE0 functionals show similar μ values of less than 1% for most Chals. The investigated compounds have a high μ values compared with many similar chalcones (Table 1) computed at different levels of theory. The μ values follow the order:

Chal1 and Chal2	$\mu_{\text{M06–2X}} < \mu_{\text{PBE0}} < \mu_{\text{ωB97X–D}} < \mu_{\text{CAM-B3LYP}} < \mu_{\text{B3LYP}}$
Chal3 and Chal4	$\mu_{\text{M06–2X}} < \mu_{\text{ωB97X–D}} < \mu_{\text{CAM-B3LYP}} < \mu_{\text{B3LYP}} < \mu_{\text{PBE0}}$
Chal5	$\mu_{\text{M06–2X}} < \mu_{\text{CAM-B3LYP}} \leq \mu_{\text{ωB97X–D}} < \mu_{\text{B3LYP}} < \mu_{\text{PBE0}}$
Chal6	$\mu_{\text{M06–2X}} < \mu_{\text{PBE0}} < \mu_{\text{B3LYP}} < \mu_{\text{ωB97X–D}} \leq \mu_{\text{CAM-B3LYP}}$
Chal7	$\mu_{\text{M06–2X}} < \mu_{\text{CAM-B3LYP}} < \mu_{\text{ωB97X–D}} < \mu_{\text{B3LYP}} \leq \mu_{\text{PBE0}}$
$\mu_{\text{Chal4}} < \mu_{\text{Chal6}} < \mu_{\text{Chal1}} < \mu_{\text{Chal2}} < \mu_{\text{Chal7}} < \mu_{\text{Chal3}} < \mu_{\text{Chal5}}$	

The μ values converge for each Chal individually, whereas Chal5 has the strongest μ, Chal4 has the lowest μ, where the substitutions were introduced on both aryl rings. Chal5 exhibits one methoxy group OCH_3 and a chlorine Cl atom, while Chal4 has two OCH_3. We notice that the two OCH_3 as terminal groups in Chal4 reduced the quantity of partial positive and negative charges in this molecule and the separations between these charges. In the case of Chal5, the high μ values can be explained by the presence of a Cl atom and one OCH_3 on both aryl rings as a powerful electron-withdrawing group with strong Pauling electronegativity and vacant 3*d* orbitals [51] and one OCH_3 as an electron-donating group. Zhao et al. [51] studied some of the inherent characteristics of the Cl atom and compared them with those of the fluorine (F) atom. Their results [51] showed that Cl atoms can form strong noncovalent interactions; therefore, intense μ. Salim et al. [52] have observed a general increase in μ values of pyrazoline analogues with Cl and F atoms as an electron-attractor group. Zhang et al. [53] found that in Cl-modified non-fullerene acceptors, the μ rises from 2.26 to 2.77 D when F atoms are substituted with Cl atoms. The results showed that, like our Chal5, electron donor–acceptor groups on opposite sides of the Chal form the basis for constructing strong NLO organic materials. Chal3 has a higher μ than Chal1, Chal2, Chal4, Chal6, and Chal7. In the case of Chal2 and Chal3, the substitutions were introduced in the benzaldehyde ring (A position) (Scheme 1). Chal2 contains an electron-withdrawing F atom, whereas Chal3 possesses a high electron-donating NH_2 at the para position (Table 1 and Fig. 3). Electron-donating groups can increase the electron density in the vicinity, potentially influencing the μ [54]. In contrast, electron-withdrawing groups may decrease electron density. The lower μ value of Chal6 compared to Chal7 could be related to electron-donating and electron-withdrawing power. Chal6 is a bromo-substituted chalcone, and Chal7 displays a furane in ring B and a chloroarene at the benzaldehyde ring. Chal1represents the non-substituted pattern. The decrease of μ values by more than 50% in Chal4 and Chal6 proves the low intramolecular charge transfer, which occurs due to the push–pull of electrons between donor and

Table 1 μ, $\langle\alpha\rangle$, $\Delta\alpha$, $\beta_{//}$, β_{tot}, β_{HRS}, and *DR* for Chal1–Chal7 obtained using five DFT levels at the 6-311+G** basis set

	μ	$\langle\alpha\rangle$	$\Delta\alpha$	$\beta_{//}$	β_{tot}	$\beta_{HRS}(DR)$
Chal1						
B3LYP	3.22	198.46	178.60	–718.21	1565.05	838.25 (3.15)
PBE0	3.13	206.65	193.71	–847.54	1817.84	902.23 (3.01)
ωB97X-D	3.14	189.21	162.35	–536.48	1193.24	600.74 (3.13)
CAM-B3LYP	3.16	190.27	163.47	–566.65	1264.65	632.58 (3.12)
M06-2X	3.06	187.60	162.52	–568.41	1286.31	632.40 (3.10)
Exp						1158.74
		180.80[d]				
		124.87[d]				
Chal2						
B3LYP	3.58	199.30	178.05	–776.21	1335.41	770.24 (2.57)
PBE0	3.40	208.66	194.05	–828.57	1484.54	863.58 (2.47)
ωB97X-D	3.47	190.26	163.19	–617.87	1043.25	602.21 (2.50)
CAM-B3LYP	3.50	190.92	163.91	–653.48	1103.78	631.58 (2.80)
M06-2X	3.38	188.01	162.26	–674.56	1125.32	612.95 (2.80)
Exp						1969.87
		180.80[d]			1597.99[c]	
		124.87[d]				
Chal3						
B3LYP	4.24	219.50	240.12	–1402.32	2764.21	1363.56 (3.24)
PBE0	4.38	232.12	270.05	–2020.45	4183.65	1930.48 (3.70)
ωB97X-D	4.10	206.65	211.16	–913.78	1673.95	902.32 (3.20)
CAM-B3LYP	4.11	208.01	213.26	–967.01	1782.35	952.34 (3.20)
M06-2X	4.06	205.66	211.25	–983.47	1810.32	957.07 (3.10)
Exp						5330.24
		217.00[e]			3583.18[d]	
		262.00[e]				
Chal4						
B3LYP	1.87	252.74	289.91	–1989.01	3337.54	1702.10 (3.06)
PBE0	2.04	269.60	331.26	–2359.65	3948.64	2049.65 (3.00)
ωB97X-D	1.66	236.60	253.77	–1528.87	2577.32	1301.25 (3.00)
CAM-B3LYP	1.67	239.03	256.46	–1606.54	2721.56	1370.58 (3.10)
M06-2X	1.60	236.65	253.64	–1617.65	2752.95	1396.58 (3.01)
Exp[a]						1853.57
		217.00[e]			3583.18[d]	
		262.00[e]				
Chal5						
B3LYP	5.14	246.30	281.58	–2717.54	4590.70	2150.65 (3.10)
PBE0	5.38	261.30	318.52	–3575.87	5766.25	2651.23 (3.06)
ωB97X-D	4.92	231.89	247.54	–1992.35	3384.65	1558.54 (3.11)
CAM-B3LYP	4.91	232.60	250.30	–2123.56	3595.64	1650.52 (3.14)
M06-2X	4.92	231.70	247.54	–1992.65	3384.98	1558.69 (3.06)
Exp						2549.25
	4.58[a]	217.00[e]		4388[a]	3583.18[d]	
	4.56[b]	262.00[e]		1025[b]		
	4.89[b]					
	5.19[c]					
Chal6						
B3LYP	2.54	228.51	195.28	–136.70	3333.54	1510.20 (3.87)
PBE0	2.45	239.59	213.13	–257.87	4842.56	2148.36 (3.24)
ωB97X-D	2.55	216.01	177.92	–3.19	2103.48	971.30 (3.20)

Table 1 (continued)

	μ	$\langle\alpha\rangle$	$\Delta\alpha$	$\beta_{//}$	β_{tot}	$\beta_{HRS}(DR)$
CAM-B3LYP	2.56	216.96	178.75	–33.56	2243.01	1034.05 (3.11)
M06-2X	2.51	214.31	177.87	50.91	2325.56	1062.27 (3.02)
Exp						2501.21
	2.55[a]	217.00[e]			3583.18[d]	
		262.00[e]				
Chal7						
B3LYP	4.20	200.64	225.95	–1083.42	1982.94	896.65 (2.95)
PBE0	4.20	210.50	249.60	–937.98	2022.22	1222.23 (2.92)
ωB97X-D	4.07	189.13	201.56	–1048.41	1810.45	966.54 (2.94)
CAM-B3LYP	4.06	190.29	202.41	–1067.32	1846.56	981.24 (2.96)
M06-2X	3.98	188.33	200.95	–1167.87	1986.01	1029.64 (2.95)
Exp						1390.54
		217.00[e]				
		262.00[e]				

Comparisons with experimental and the DFT results

[a][31] Results of similar Chals obtained at the LC-ωPBE level

[b][55] Experimental value for urea

[c][30] Results for (1E,4E)-1,5-di-p-tolylpenta-1,4-dien-3-one obtained at the B3LYP level

[d][56] Results for chalcone and 2,3,4,4'-tetramethoxychalcone obtained at the CAM-B3LYP level

[e][57] Results for the (2E)-3-(4-methylphenyl)-1-(3-nitrophenyl)prop-2-en-1-one and (2E)-3-[4- (dimethylamino)phenyl]-1-(3-nitrophenyl)prop-2-en-1-one calculated at the PBE0 level

[29] Experimental β_{HRS} result of Chals

attractor units. Introducing Cl with strong electronegativity can affect the electron density distribution along the conjugated backbone of all Chals. Hence, the type, number, and position of these units are what generate a clear variation in μ.

Polarizability

This section scrutinizes the B3LYP, PBE0, ωB97X-D, CAM-B3LYP, and M06-2X α results. The calculated mean polarizability $\langle\alpha\rangle$ and polarizability anisotropy $\Delta\alpha$ of the selected Chal1–Chal7 are presented in Figs. 4 and 5. The PBE0 method shows the highest α values. Their $\langle\alpha\rangle$ and $\Delta\alpha$ varied between (206.65 to 269.60) and (193.71 to 331.26 a.u.). Cha4 gets the highest $\langle\alpha\rangle$ and $\Delta\alpha$ varied between (236.60 and 269.60) and (253.77 and 331.26 a.u.) obtained at the ωB97X-D and PBE0 levels, respectively. Theoretical studies [58–62] showed that the PBE0 gives high α compared to some functionals. Chal1 without substitution gets the lowest $\langle\alpha\rangle$ and $\Delta\alpha$. In this case $\langle\alpha\rangle$ and $\Delta\alpha$ are 187.60 and 162.35 a.u. at the M06-2X and ωB97X-D, respectively. A careful analysis of α components of these Chals shows that the contributions along the x and y axis (α_{xx} and α_{yy}) are the majority. The calculated α showed that the Chals size drove the average polarizability, and $\Delta\alpha$ depends on the nature of each Chals. Several α studies [63–67] show the same relationship. Andrade-Filho and co-workers [56] proposed new metabolites chalcone with $\langle\alpha\rangle$ between 37×10^{-24} and 53.5×10^{-24} esu, which are quite similar than those of the selected Chal1 and Chal2. The authors showed that the structural effect of the substitution of HC=CH by $H_2C–CH_2$ acts decreasing $\langle\alpha\rangle$. Proposed new chemicals which are the (2E)-3-(4-methylphenyl)-1-(3-nitrophenyl)prop-2-en-1-one and (2E)-3-[4-(dimethylamino)phenyl]-1-(3-nitrophenyl) prop-2-en-1-one [57] with $\langle\alpha\rangle$ between 32.15×10^{-24} and 38.76×10^{-24} esu, respectively, similar to those of selected Chals in this new study.

Hyperpolarizability

Hyperpolarizabilities $\beta_{//}$, β_{tot}, β_{HRS}, and DR of chalcone-based derivatives Chal1–Chal7 are computed and presented in Table 1, Figs. 7 and 8. The obtained hyperpolarizability contributions show that the β ones along the x-axis are the majority (Fig. 6). High β_{tot} values are obtained for these Chals. The β_{tot} values ranged from 1484.54 to 5766.25 a.u. using the PBE0 level. This approach gives the highest β_{tot} values of all studied Chals compared to other DFT levels B3LYP, M06-2X, CAM-B3LYP, and ωB97X–D used in this investigation while the ωB97X–D functional with 22% of HF exchange level gives the lowest β_{tot} values. The functionals B3LYP give close β_{tot} values to that of PBE0. The

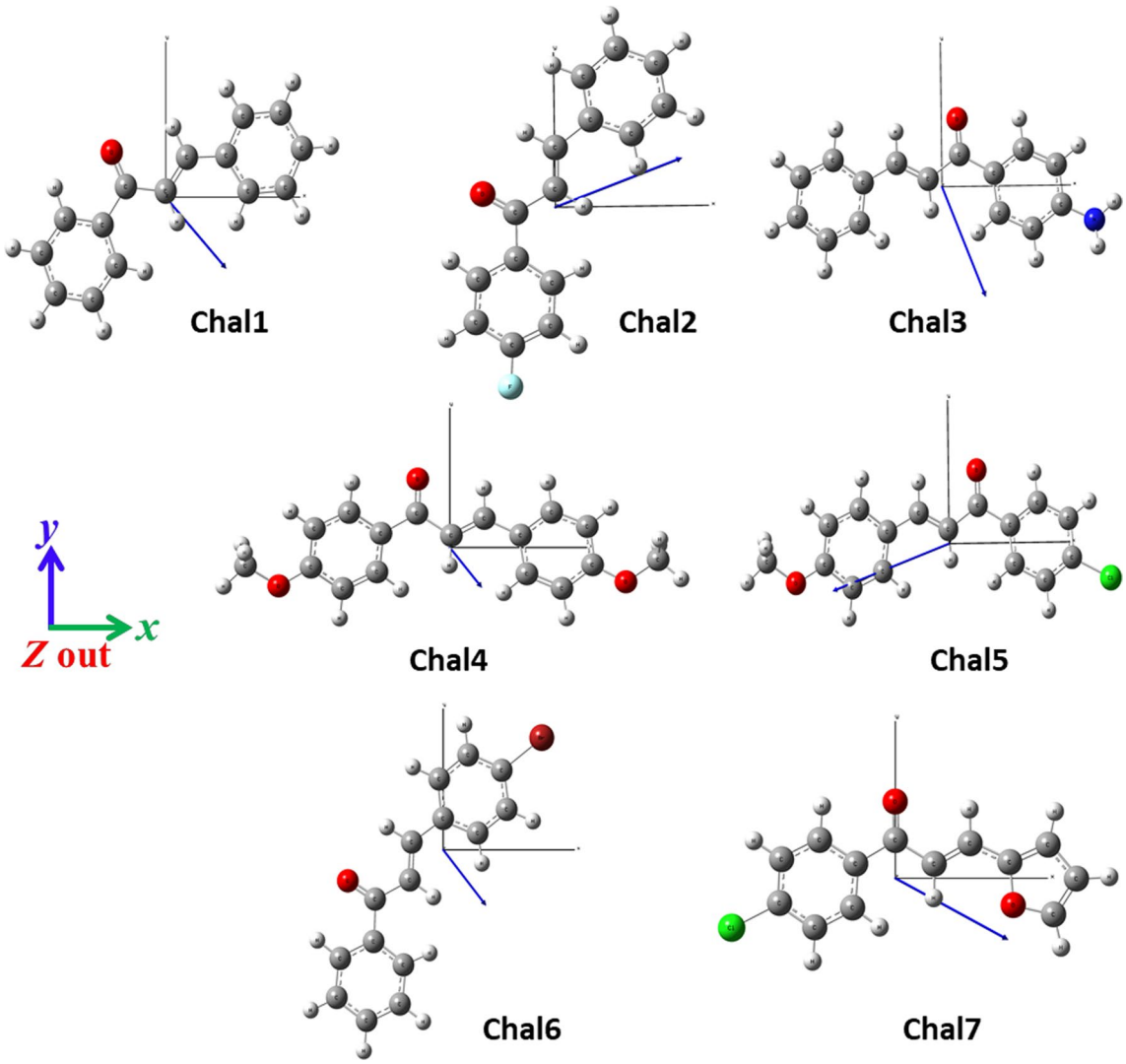

Fig. 2 μ vector of Chal1–Chal7

difference does not exceed 13.90, 10.04, 33.92, 15.47, 20.38, 31.16, and 1.94% for Chal1, Chal2, Chal3, Chal4, Chal5, Chal6, and Chal7, respectively (Table 1). The variation of β_{tot} as a function of the DFT functionals attains a maximum of ~ 34% for Chal1, ~ 30% for Chal2, ~ 60% for Chal3, ~ 41% for Chal5, ~ 57% for Chal6, and ~ 11% for Chal7. For the $\beta_{//}$, the highest and the lowest values are –3.19 and –3575.87 a.u., respectively, which were obtained using the ωB97X–D and PBE0 functionals, respectively. The same behavior was also found for [68–70]. These findings lead to the following orderings:

Chal1-Chal7 $\beta_{tot\ \omega B97X-D} < \beta_{tot\ CAM-B3LYP} < \beta_{tot\ M06-2X} < \beta_{tot\ B3LYP} < \beta_{tot\ PBE0}$

β_{tot} Chal2 < Chal1 < Chal7 < Chal4 < Chal3 < Chal6 < Chal5.

In this section, we also investigated the correlation between the Chal structures and the second-order NLO responses β_{HRS} and $\beta_{//}$. The relationship between the β_{HRS} and $\beta_{//}$ may depend on the specific characteristics of the Chals (electronic structure) under investigation. Researchers typically use a combination of experimental measurements and computational simulations, like our study, to understand better the NLO properties and the connection between different β. A comparative study of selected Chal1–Chal7 indicates that the higher β_{HRS} values were obtained for these Chals using hybrid DFT functionals, including a minor fraction of the Hartree–Fock (HF) exchange. Whereas the XC functionals containing larger amounts of HF exchange, such as M06-2X, ωB97X-D, and CAM-B3LYP, give the lowest β_{HRS} values. The CAM-B3LYP, M06-2X, and ωB97X-D

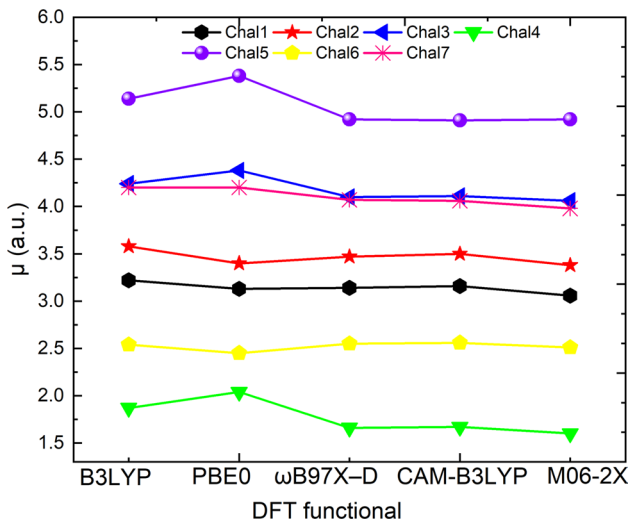

Fig. 3 μ of Chal1–Chal7 calculated using five functionals at the 6-311+G** basis set

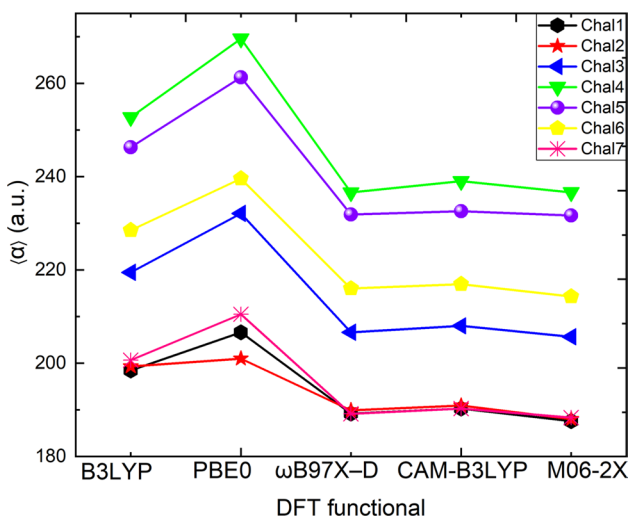

Fig. 4 $\langle\alpha\rangle$ of Chal1–Chal7 calculated using five levels at the 6-311+G** basis set

values are convergent and smaller than the B3LYP, which contains the smallest amount of HF exchange. The B3LYP and PBE0 functional with 20% and 40% HF exchange gives the highest β_{HRS} values equal to 2150.65 and 2651.23 a.u, respectively, whereas the ωB97X-D DFT global hybrid functional with 22% HF exchange yields the smallest β_{HRS} values equal 600.74, 602.21, 902.32, 1301.25, 1558.54, and 971.30 a.u. for Chal1, Chal2, Chal3, Chal4, Chal5, and Chal6, respectively. As an exception, the B3LYP gives the lowest β_{HRS} values for Chal7 (896.65 a.u). In the meantime, the PBE0 functional yields the greatest β_{HRS} values equal to 902.23, 863.58, 1930.48, 2049.65, 2651.23, 2148.36, and 1222.23 a.u. for Chal1, Chal2, Chal3, Chal4, Chal5, Chal6,

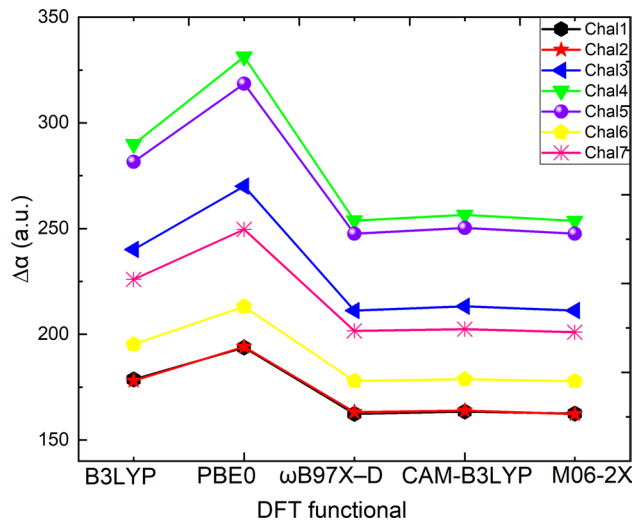

Fig. 5 $\Delta\alpha$ of Chal1–Chal7 calculated using five levels at the 6-311+G** basis set

and Chal7, respectively. A glance at Table 1, Figs. 7 and 8 is enough to determine that we state opposite variations between the β_{HRS} and $\beta_{//}$ in addition to the presence of a direct correlation between the β_{HRS} and β_{tot}. Many studies [71] have reached the same findings. Computations lead us to propose an increasing/decreasing classification relative to the β_{HRS} and $\beta_{//}$, respectively. The established order is as follows:

Chal1, Chal2, Chal4 and Chal5	$\beta_{HRS\ \omega B97X-D} < \beta_{HRS\ M06-2X} < \beta_{HRS\ CAM-B3LYP} < \beta_{HRS\ B3LYP} < \beta_{HRS\ PBE0}$
Chal1, Chal3 and Chal6	$\beta_{HRS\ \omega B97X-D} < \beta_{HRS\ CAM-B3LYP} < \beta_{HRS\ M06-2X} < \beta_{HRS\ B3LYP} < \beta_{HRS\ PBE0}$
Chal7	$\beta_{HRS\ B3LYP} < \beta_{HRS\ \omega B97X-D} < \beta_{HRS\ CAM-B3LYP} < \beta_{HRS\ M06-2X} < \beta_{HRS\ PBE0}$
β_{HRS}	Chal2 < Chal1 < Chal7 < Chal3 < Chal4 < Chal6 < Chal5
Chal1, Chal2, Chal3 and Chal4	$\beta_{//\ \omega B97X-D} > \beta_{//\ M06-2X} > \beta_{//\ CAM-B3LYP} > \beta_{//\ B3LYP} > \beta_{//\ PBE0}$
Chal5	$\beta_{//\ \omega B97X-D} > \beta_{//\ M06-2X} > \beta_{//\ CAM-B3LYP} > \beta_{//\ B3LYP} > \beta_{//\ PBE0}$
Chal6	$\beta_{//\ M06-2X} > \beta_{//\ \omega B97X-D} > \beta_{//\ CAM-B3LYP} > \beta_{//\ B3LYP} > \beta_{//\ PBE0}$
Chal7	$\beta_{//\ PBE0} > \beta_{//\ \omega B97X-D} > \beta_{//\ CAM-B3LYP} > \beta_{//\ M06-2X} > \beta_{//\ B3LYP}$
$\beta_{//}$	Chal6 > Chal1 > Chal7 > Chal3 > Chal4 > Chal5

Our computations show that electron donating and withdrawing groups can effectively increase and decrease the first hyperpolarizability β, respectively. The results in Tables 1

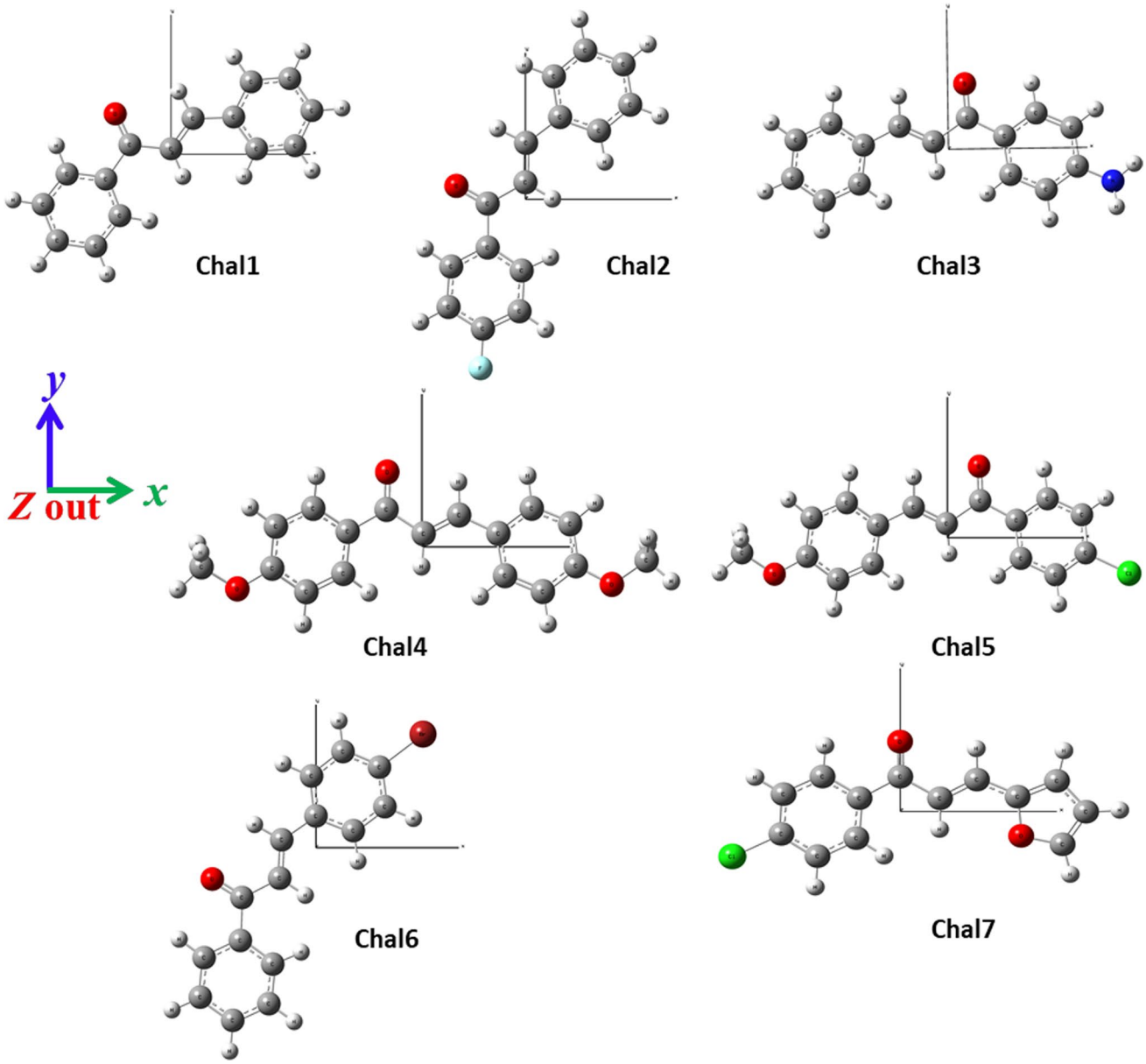

Fig. 6 Chal1–Chal7 orientation during calculations

and 2 establish the influence of different substituents and signify the importance of position and substitution number on the β Chals. The values are the largest for the disubstituted Chal5 than the mono-substituted ones. $\beta_{HRS}(OCH_3/Cl)_{Chal5} > \beta_{HRS}(Br)_{Chal6} > \beta_{HRS}(NH_2)_{Chal3} > \beta_{HRS}(F)_{Chal2}$. $\beta_{tot}(OCH_3/Cl)_{Chal5} > \beta_{tot}(Br)_{Chal6} > \beta_{tot}(NH_2)_{Chal3} > \beta_{tot}(F)_{Chal2}$. These high β_{HRS} and β_{tot} values are due to the electron transfer from the electron-donating OCH_3 via the Chals to the electron-withdrawing Cl. These values decrease significantly in the absence of electron-donating or/and electron-withdrawing group (D-π-(A or D) and A-π-(A or D)) as illustrated by Chal4 with two OCH_3. Chal1 represents the non-substituted pattern, and Chal7, with the furane in rings B and A, has a chloroarene at the benzaldehyde ring. The β values are influenced by the distribution of electrons within a molecule. Electron-donating groups, by increasing electron density, and electron-withdrawing groups, by decreasing electron density, can affect the NLO response without ignoring the role of the overall molecular architecture (the HC=CH bridge π-character). The effectiveness of the targeted compounds as the basis for constructing effective NLO organic materials can be confirmed by comparison to other studies (Table 1). β_{tot} values of Chal5 are nearly five times higher than that of para-nitroaniline *p*-NA and one hundred and thirty-five times greater than that reported for urea [55] as well-known prototype NLO molecules add to

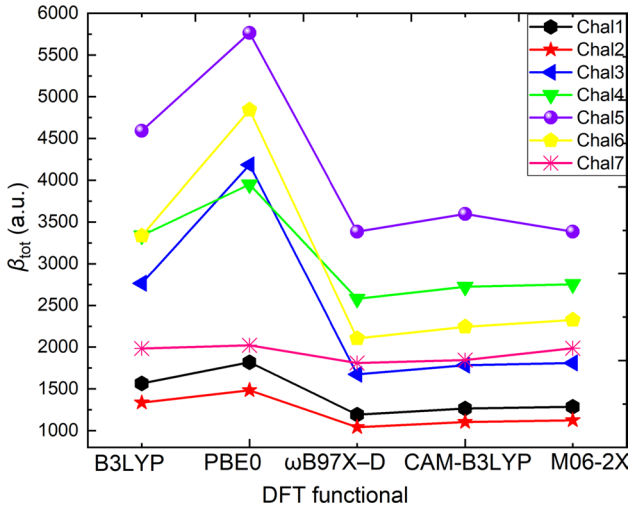

Fig. 7 β_{tot} of Chal1–Chal7 calculated using five levels at the 6-311+G** basis set

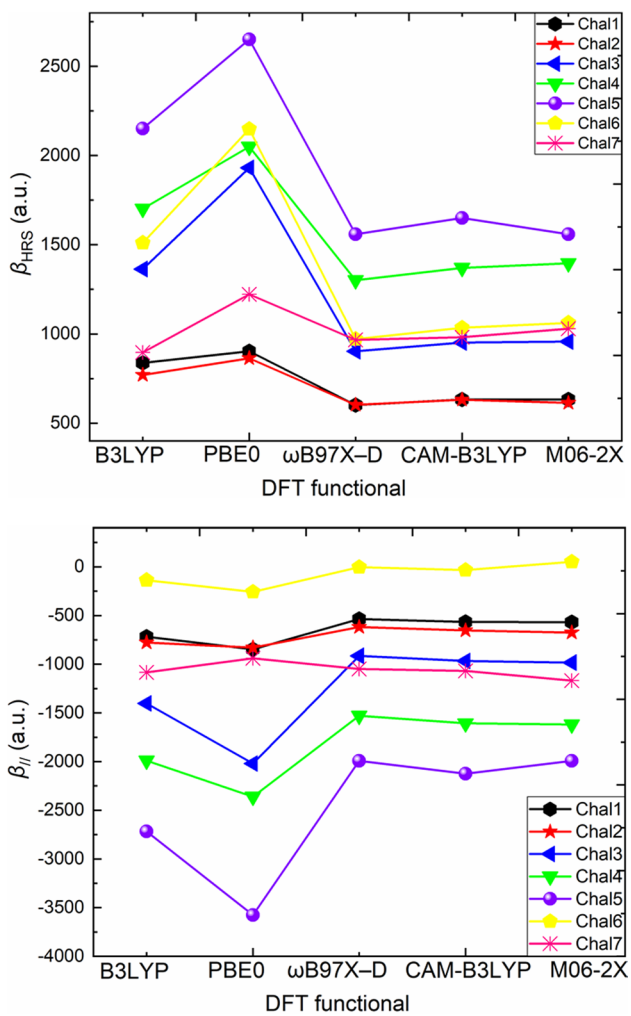

Fig. 8 $\beta_{//}$ and β_{HRS} of Chal1–Chal7 calculated using five levels at the 6-311+G** basis set

Table 2 E_{HOMO}, E_{LUMO}, E_g in eV and β_{tot} in a.u. of Chal1–Chal7 derivatives obtained using five DFT levels at the 6-311+G** basis set

	E_{HOMO}	E_{LUMO}	E_g	β_{tot}
Chal1				
B3LYP	–6.64	–2.51	4.13	1565.05
PBE0	–5.60	–2.43	3.17	1817.84
ωB97X–D	–5.61	–0.19	5.42	1193.24
CAM-B3LYP	–7.80	–2.08	5.72	1264.65
M06-2X	–8.00	–2.33	5.67	1286.31
Chal2				
B3LYP	–6.73	–1.91	4.13	1335.41
PBE0	–6.60	–3.52	3.08	1484.54
ωB97X–D	–6.54	–1.15	5.39	1043.25
CAM-B3LYP	–6.56	–0.86	5.88	1103.78
M06-2X	–6.76	–1.19	5.57	1125.32
Chal3				
B3LYP	–6.04	–2.60	3.44	2764.21
PBE0	–5.69	–3.51	2.18	4183.65
ωB97X–D	–5.77	–0.28	5.49	1673.95
CAM-B3LYP	–6.84	–1.19	5.65	1782.35
M06-2X	–7.38	–1.83	5.55	1810.32
Chal4				
B3LYP	–6.05	–2.16	3.89	3337.54
PBE0	–5.67	–3.50	2.17	3948.64
ωB97X–D	–5.75	–1.27	4.48	2577.32
CAM-B3LYP	–6.82	–0.95	5.87	2721.56
M06-2X	–7.36	–1.82	5.54	2752.95
Chal5				
B3LYP	–6.44	–2.70	3.74	4590.70
PBE0	–5.68	–3.52	2.16	5766.25
ωB97X–D	–5.76	–1.29	4.47	3384.65
CAM-B3LYP	–6.83	–1.76	5.07	3595.64
M06-2X	–7.36	–1.84	5.52	3384.98
Chal6				
B3LYP	–6.71	–2.64	4.07	3333.54
PBE0	–5.61	–3.46	2.15	4842.56
ωB97X–D	–5.71	–1.26	4.45	2103.48
CAM-B3LYP	–6.80	–0.95	5.85	2243.01
M06-2X	–7.31	–1.62	5.69	2325.56
Chal7				
B3LYP	–6.64	–2.66	3.98	1982.94
PBE0	–5.65	–2.50	3.15	2022.22
ωB97X–D	–5.70	–0.23	5.47	1810.45
CAM-B3LYP	–6.93	–0.33	6.10	1846.56
M06-2X	–7.15	–1.45	5.70	1986.01

that all targeted Chals in the present investigation possess larger β_{tot} values compared to that of *p*-NA. Most importantly, among all Chal1–Chal7; Chal5 has a high β_{tot} value compared with those of similar chalcone derivatives [57] designed with rotation of OCH_3 at three different possible

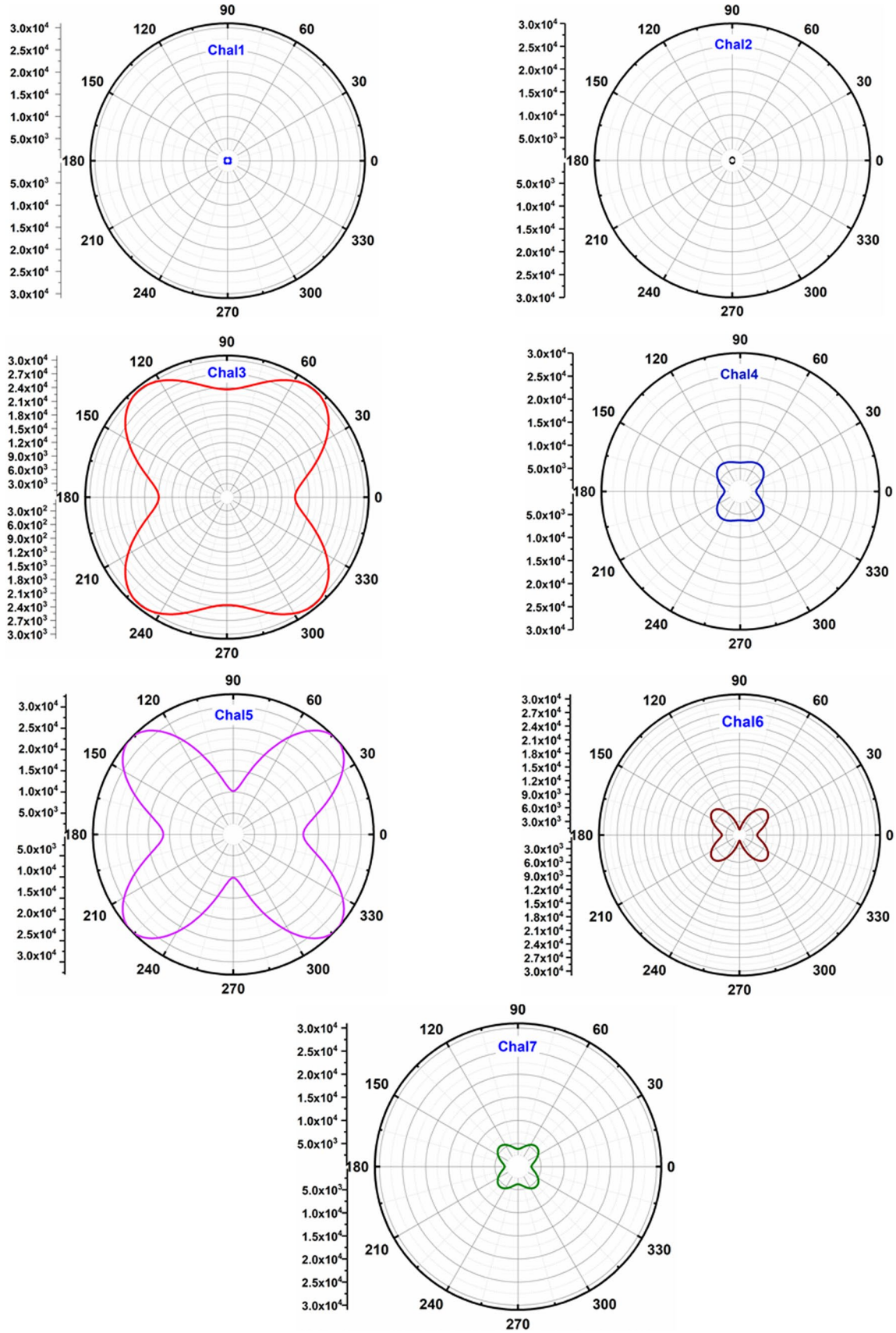

Fig. 9 $I_{\Psi V}^{2\omega}$ in a.u. of Chal1–Chal7 as a function of Ψ at 1064 nm obtained with the B3LYP/6-311+G** level

ortho, meta, and para positions on the phenyl ring. In addition, Chals have high β_{tot} values compared with those of some Chals biotransformed using the endophytic fungus Aspergillus flavus (an agent naturally found in the Amazon biome), 2,3,4,4′-tetramethoxychalcone [56] obtained at the CAM-B3LYP/6-311++G** level, and (1E,4E)-1,5-di-p-tolylpenta-1,4-dien-3-one obtained at the B3LYP/6-31G level of theory [30].

The four DFT functionals used in this study give close *DR* values for the selected Chal1-Chal7. Their *DR* values were close to 3. The *DR* results, in combination with the chemical topology of the Chal structures, are congruent with the representative C_s the molecular point group of these Chals. The C_s point group symmetry is well marked by the presence of a single σ plane of symmetry (a planar structure) for this type of Chals. The *DR* property covers a broad range of dipolar-octupolar characters of our Chals and makes it possible to know the symmetry of the Chals when it has a few elements of the non-zero β tensor. The evolution of $I^{2\omega}_{\Psi V}$ with respect to the elliptical polarization of the incident light denoted by the polarization angle Ψ of the incident beam was also investigated in this study. To further understand the β_{HRS} results, we show the calculated $I^{2\omega}_{\Psi V}$ at the PBE0 functional (Fig. 9). $I^{2\omega}_{\Psi V}$ intensity corresponding to the Ψ varied from –180 to 180° with a step-size of 1°, their shapes agree quantitatively with the more polar Chal3 and Chal5. The results show that the trends of $I^{2\omega}_{\Psi V}$ are completely consistent with the β_{HRS} of Chlas. The same assessment has been obtained by Lu et al. [72] for the 1,3-thiazolium-5-thiolates mesoionic.

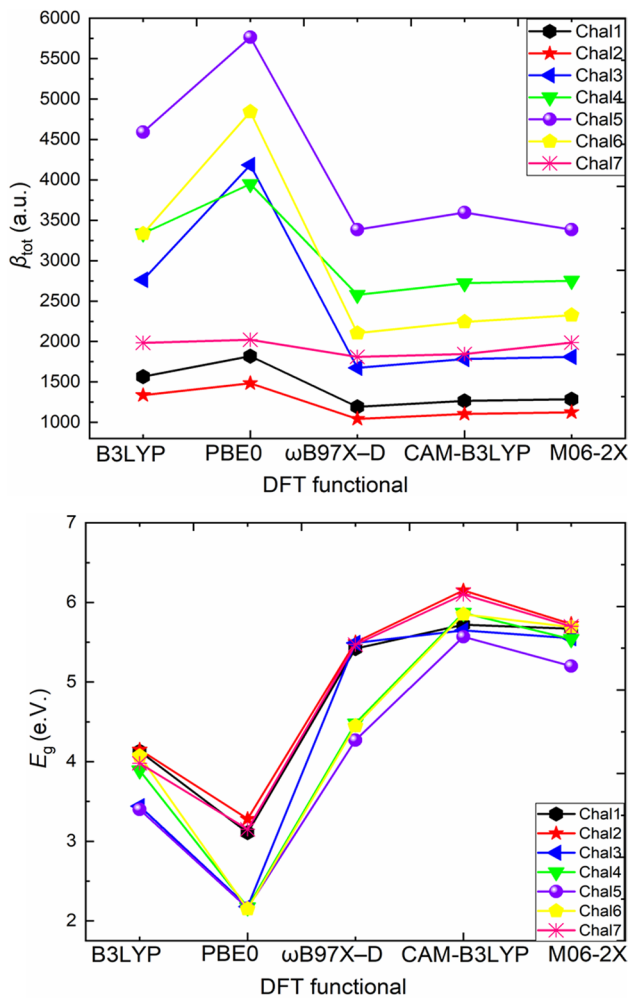

Fig. 10 β_{tot} (upper panel) and E_g (lower panel) of Chal1–Chal7 calculated using five levels at the 6-311+G** basis set

Molecular orbitals analysis and their energy gaps

The FMO analysis provides valuable insights into the electronic structure, reactivity, and properties of molecules, serving as a fundamental tool for advancing our understanding of chemical phenomena and guiding the rational design of new materials and processes [16, 73–75]. Frontier electron density predicts the most reactive position in π-electron systems and clarifies several types of reactions in conjugated systems [38, 76]. Compounds exhibiting a significant E_g demonstrate stability, hence exhibiting greater chemical hardness than those with a smaller E_g [77, 78]. The study of the occupied and the virtual orbitals helps provide more information about energy gaps E_g, orbital surfaces, and the possibility of the charge for Chals. Table 2 and Figs. 10 and 11 summarize the E_{HOMO}, E_{LUMO} and their E_g for Chals. The substituent effect on FMOs is straightforward; the NH_2 and OCH_3 donor groups cause increasing orbital energy, while the Cl and Br acceptor groups cause decreasing orbital energy. The DFT E_g results show that the PBE0 gives the lowest E_g values compared to the B3LYP, ωB97X–D, CAM-B3LYP, and M06-2X levels. Their values are 3.17, 3.08, 2.18, 2.17, 2.16, 2.15, and 3.15 eV for Chal1, Chal2, Chal3, Chal4, Chal5, Chal6, and Chal7, respectively. Also, the B3LYP gives low E_g values compared to ωB97X–D, CAM-B3LYP, and M06-2X levels. Their values are 4.13, 4.13, 3.44, 3.89, 3.74, 4.07, and 3.98 eV for Chal1, Chal2, Chal3, Chal4, Chal5, Chal6, and Chal7, respectively. Recent studies [68–71, 79–82] show the suitability of the PBE0 for the E_g calculation. For similar Chals [83], the PBE0 provide reliable E_g. Their calculated values range from 3 to 4 eV for the (E)-1-(5-bromo-2-thienyl)-3-(4-bromophenyl)prop-2-en-1-one,(E)-1-(5-bromo-2-thienyl)-3-(3-chlorophenyl) prop-2-en-1-one, and (E)-1-(5-bromo-2-thienyl)-3-(2-methoxyphenyl)prop-2-en-1-one [84], the B3LYP level gives similar E_g values [85] ranged between 3.71 and 3.93 eV. The ωB97X–D method overestimates E_g values compared to the B3LYP and PBE0. Their obtained values are 5.42, 5.39, 5.49, 5.48, 5.47, and 4.47 eV, respectively. These high E_g values may be due to the dispersion effect at the ωB97X–D level compared to some DFT functionals [54, 86, 87]. The

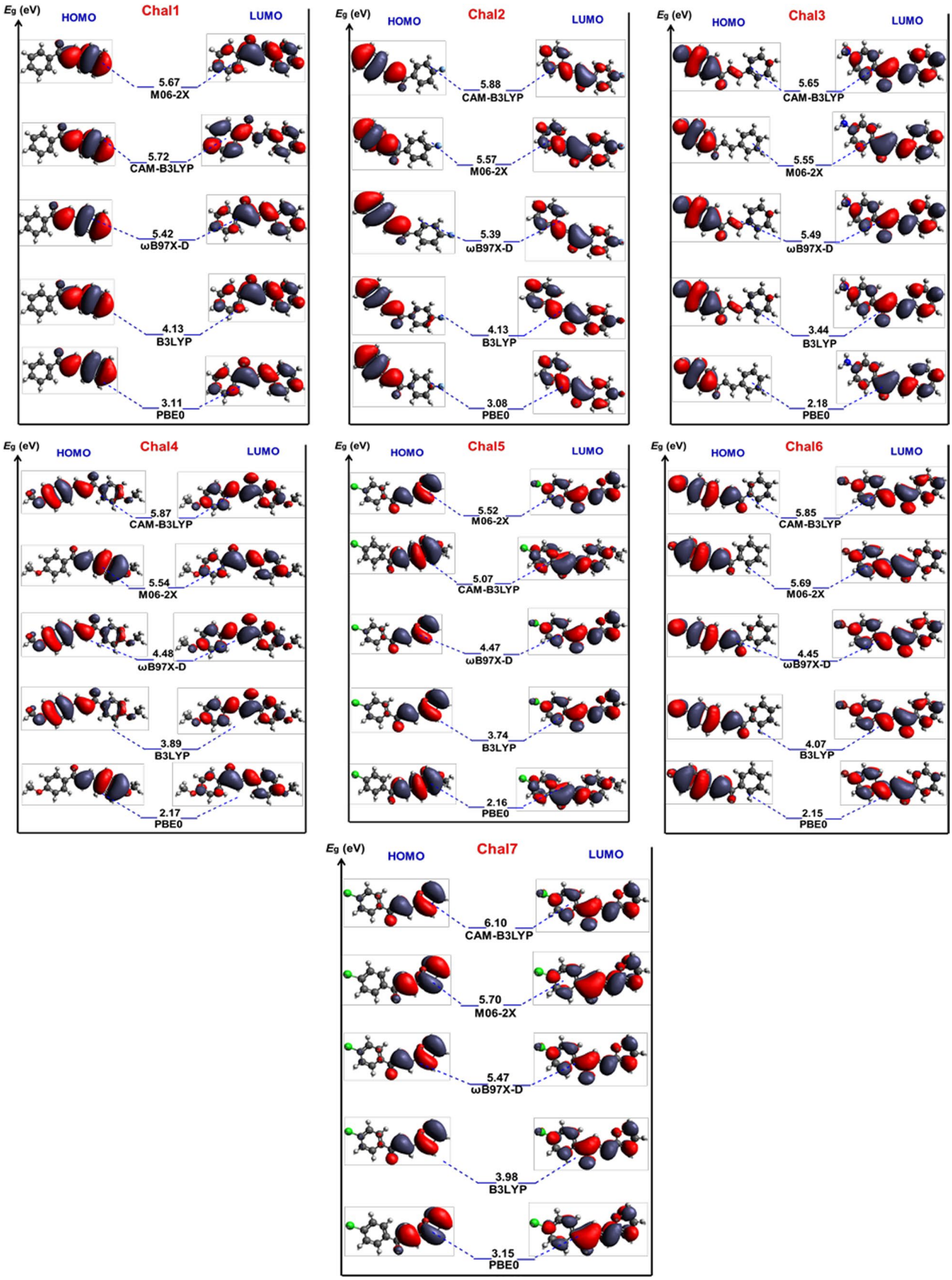

Fig. 11 HOMO, LUMO, and E_g in eV of Chal1–Chal7 estimated by five DFT functionals

substitution with NH_2 in the case of Chal3 decreases the E_g with 1 eV compared to Chal1 at the PBE0 level.E_g showed the same variation in the case of Chal4, where the OCH_3 group was present. The presence of the push–pull system, which is represented by the OCH_3 as donor and Cl as attractor (Chal5), decreases the E_g value and increases the β_{tot} by 68.48% compared to Chal1, which confirms the significant effect of the donor–acceptor group on enhancing the NLO properties. The presence the Br in the case of Chal6 decreases the E_g value and increase considerably the β_{tot} by 62.42% compared to Chal1. In the case of Chal7 or the presence of Cl alone, a slight decrease in the E_g followed by a significant increase in β_{tot}, but not like the other Chals, clearly shows the crucial effect of the substitution on the E_g and NLO properties. Study [49] highlighted the chlorination influence on the photophysical and photovoltaic properties and the decreasing effect of both HOMO and LUMO simultaneously in donor and acceptor molecules. The presence of donor and attractor electron groups alters the nature of delocalization and consequently affects the electronic properties of the Chals [83]. The analysis of FMO surfaces shows that the HOMOs of Chals are more localized on the cinnamoyl group (Fig. 11), whereas strong delocalization over the whole Chals was shown in the LUMO isosurfaces. The same distribution was demonstrated by Xue et al. [83] for similar Chals, and in the biphenyl based difluorochalcones ((2E)-1-[4-(2,4-difluorophenyl)phenyl]3-arylprop 2-en-1-ones) [88]. The FMO isosurfaces of the selected Chals demonstrate the π-type MO characteristics (Fig. 11). Similar Chals [69] demonstrate the same orbital natures. For this type of Chals, the relatively small E_g obtained at the PBE0 approach and high dipole moments contribute to high NLO responses. Changes in the electronic structure, such as alterations in orbital energies or the presence of electronic states near the band edges, can influence both binding energy and E_g. The functional groups that donate or withdraw electrons can affect both its binding affinity and the energy levels of molecular orbitals [89–94].

To bolster our noticed trends in linear properties and NLO properties (E_{HOMO}, E_{LUMO}, E_g, μ and α, and β) as well as in NLO properties (β). Here, we have correlated our observed results for linear and NLO properties with the global relativity descriptors of Chal5, such as chemical hardness (η) [95], chemical potential (μ), chemical softness (S), electronegativity (χ), electrophilic index (ω), and nucleophilicity index (N) [96, 97] (Table 3). The small E_g of Chal5 (2.16 eV) indicates that charge transfer easily occurs in it, which influences the biological activity of the molecules [98]. While the E_{HOMO} and E_{LUMO} values are all negative, confirming this derivative's stability [99]. A molecule with a small E_g is more polarized and characterized by good bioactivity, high chemical reactivity, and low kinetic stability, known as a soft molecule [100, 101]. The stability of Chal5 is validated by the chemical hardness, which is 2.76 eV. The computed significant η value and the small E_g value for Chal5 exhibits promising charge transfer in this Chal. ω represents the energy reduction measure caused by the maximum charge transfer between the acceptor and donor [102]. ω is related to the stabilization of energy when the system gains an additional electronic charge from the surroundings and quantifies the global electrophilic power of the molecule [103]. These descriptors were evaluated from the following equations:

$$A = -E_{LUMO}; I = -E_{HOMO}; V = (I + A)/2; S = 1/2\eta$$
$$\eta = (-A + I)/2; \chi = (I + A)/2; \omega = V^2/2\eta; N = 1/\omega$$

According to the absolute scale of electrophilicity based on the ω index, Chal5 may be classified as strong electrophiles with $\omega > 1.5$ eV, moderate electrophiles with $0.8 < \omega < 1.5$ eV, and marginal electrophiles with $\omega < 0.8$ eV [104]. The higher values of ω described Chal5 as a good electrophile. The strong electrophilic nature of Chal5 supports their usability as bioactive substances [105]. For this purpose this part has been added, as this information will be valuable for examining the biological activity of Chal5 for its exciting NLO properties.

Conclusion

The current study describes for the first time seven chalcone-based derivatives where the substituent has a significant electronic effect that modulates some overall molecular properties (μ, α, β, and E_g), which was corroborated by combining theoretical results. Various factors, including molecular geometry, position, number of substitutions, and choice of computational level, influence the NLO

Table 3 E_{HOMO}, E_{LUMO}, E_g, I, A, η, χ, ω in eV, S, V, and N in eV^{-1} of Chal5 computed at five DFT approaches using the 6-311+G** basis set

	E_{HOMO}	E_{LUMO}	E_g	I	A	χ	η	S	V	ω	N
B3LYP	–6.44	–2.70	3.74	6.44	2.70	4.57	1.87	0.26	–4.57	5.36	0.17
PBE0	–5.68	–3.52	2.16	5.68	3.52	4.60	1.08	0.46	–4.60	9.79	0.10
ωB97X–D	–5.76	–1.29	4.47	5.76	1.29	3.52	2.23	0.22	–3.52	2.77	0.36
CAM-B3LYP	–6.83	–1.76	5.07	6.83	1.76	4.29	2.53	0.19	–4.29	3.28	0.30
M06-2X	–7.36	–1.84	5.52	7.36	1.84	4.60	2.76	0.18	–4.60	3.83	0.26

parameters. The order of μ and α varies based on the different approximations and treatments of the electronic interactions and exchange–correlation effects implemented by each functional. Different methods have various levels of sophistication and accuracy in describing electronic interactions, giving different predictions for linear and NLO parameters. The study's functionals also differ in capturing the electronic structure and molecular interactions, leading to variations in the predicted NLO parameters. We carefully consider these factors and validate the results using multiple computational approaches (B3LYP, PBE0, M06-2X, CAM-B3LYP, and ωB97X-D) and compare them with experimental data to enhance the reliability of our findings. We found that these Chals get low E_g and possess efficient β_{tot} and β_{HRS} responses. The PBE0 functional gives the highest β_{HRS} and β_{tot} values and is the most satisfying functional for predicting the NLO properties of these Chals. Chal5 has shown superior NLO properties as compared to other selected Chals. In addition to the direct link between the β_{HRS} and β_{tot}, we also indicate the opposite variations between the β_{HRS} and $\beta_{//}$. An inverse relationship has been obtained between the β_{tot} and E_g. This quantum chemical exploration of Chals with high hyperpolarizabilities will direct numerous scientists to use computational data for rational design of novel chalcone-based materials with potential applications in optoelectronic devices, such as light-emitting diodes (LEDs) and photovoltaic cells.

Acknowledgements This investigation was supported by the Algerian Ministry of Higher Education and Scientific Research as well as the directorate general for scientific research and technological development.

Data availability Not applicable.

Declarations

Competing interests The authors declare that they have no known competing financial interests or personal relationships that could have appeared to influence the work reported in this paper.

References

1. L. Claisen, A. Claparède, Berichte Der Dtsch. Chem. Gesellschaft. **14**, 2460–2468 (1881). https://doi.org/10.1002/cber.188101402192
2. L.M.G. Abegão, R.D. Fonseca, F.A. Santos, G.B. Souza, A.L.B.S. Barreiros, M.L. Barreiros, M.A.R.C. Alencar, C.R. Mendonça, D.L. Silva, L. De Boni, J.J. Rodrigues, Second- and third-order nonlinear optical properties of unsubstituted and mono-substituted chalcones. Chem. Phys. Lett. **648**, 91–96 (2016). https://doi.org/10.1016/j.cplett.2016.02.009
3. M.S. Alam, S.M.M. Rahman, D.U. Lee, Synthesis, biological evaluation, quantitative-SAR and docking studies of novel chalcone derivatives as antibacterial and antioxidant agents. Chem. Pap. **69**, 1118–1129 (2015). https://doi.org/10.1515/chempap-2015-0113
4. J.M.F. Custodio, G.D.C.D. Oliveira, F. Gotardo, L.H.Z. Cocca, L. De Boni, C.N. Perez, L.J.Q. Maia, C. Valverde, H.B. Napolitano, F.A.P. Oso, Chalcone as potential nonlinear optical material: a combined theoretical, structural, and spectroscopic study. J. Phys. Chem. C **123**, 5931–5941 (2019). https://doi.org/10.1021/acs.jpcc.9b01063
5. S.N.A. Bukhari, M. Jasamai, I. Jantan, Synthesis and biological evaluation of chalcone derivatives (mini review). Mini-Rev. Med. Chem. **12**, 1394–1403 (2012). https://doi.org/10.2174/138955751120913 94
6. A. Detsi, M. Majdalani, C.A. Kontogiorgis, D. Hadjipavloulitina, Natural and synthetic 2'-hydroxy-chalcones and aurones: synthesis, characterization and evaluation of the antioxidant and soybean lipoxygenase inhibitory activity. Bioorg. Med. Chem. **17**, 8073–8085 (2009). https://doi.org/10.1016/j.bmc.2009.10.002
7. A.K. Babu, K. Selvaraju, Synthesis and characterization of some novel chalcone derivatives. Rasayan J. Chem. **11**, 1501–1505 (2018). https://doi.org/10.31788/RJC.2018.1144037
8. M. Xu, P. Wu, F. Shen, J. Ji, K.P. Rakesh, Bioorganic Chemistry Chalcone derivatives and their antibacterial activities: current development. Bioorg. Chem. **91**, 103133 (2019). https://doi.org/10.1016/j.bioorg.2019.103133
9. J. Wu, J. Li, Y. Cai, Y. Pan, F. Ye, Y. Zhang, Y. Zhao, S. Yang, X. Li, G. Liang, Evaluation and discovery of novel synthetic chalcone derivatives as anti-inflammatory agents. J. Med. Chem. **54**, 8110–8123 (2011). https://doi.org/10.1021/jm200946h
10. Y. Goto, A. Hayashi, Y. Kimura, M. Nakayama, Second harmonic generation and crystal growth of substituted thienyl chalcone. J. Cryst. Growth **108**, 688–698 (1991). https://doi.org/10.1016/0022-0248(91)90249-5
11. H.J. Ravindra, A. John Kiran, S.R. Nooji, S.M. Dharmaprakash, K. Chandrasekharan, B. Kalluraya, F. Rotermund, Synthesis, crystal growth and characterization of a phase matchable nonlinear optical single crystal: p-chloro dibenzylideneacetone. J. Cryst. Growth **310**, 2543–2549 (2008). https://doi.org/10.1016/j.jcrysgro.2007.12.066
12. P.C. Rajesh Kumar, V. Ravindrachary, K. Janardhana, B. Poojary, Structural and optical properties of a new chalcone single crystal. J. Cryst. Growth **354**, 182–187 (2012). https://doi.org/10.1016/j.jcrysgro.2012.06.006
13. D. Haleshappa, A. Jayarama, R. Bairy, S. Acharya, P.S. Patil, Second and third order nonlinear optical studies of a novel thiophene substituted chalcone derivative. Phys. B Condens. Matter. **555**, 125–132 (2019). https://doi.org/10.1016/j.physb.2018.11.046
14. M.R.S.A. Janjua, Photovoltaic properties and enhancement in near-infrared light absorption capabilities of acceptor materials for organic solar cell applications: a quantum chemical perspective via DFT. J. Phys. Chem. Solids **171**, 110996 (2022). https://doi.org/10.1016/j.jpcs.2022.110996
15. M.R.S.A. Janjua, Prediction and Understanding: Quantum chemical framework of transition metals enclosed in a $B_{12}N_{12}$ inorganic nanocluster for adsorption and removal of DDT from the environment. Inorg. Chem. **60**, 10837–10847 (2021). https://doi.org/10.1021/acs.inorgchem.1c01760
16. A. Irfan, M. Hussien, M.Y. Mehboob, A. Aziz, M.R.S.A. Janjua, Learning from fullerenes and predicting for Y6: machine learning and high-throughput screening of small molecule donors for organic solar cells. Energy Technol. **10**, 2101096 (2022). https://doi.org/10.1002/ente.202101096
17. M.I. Abdullah, M.R.S.A. Janjua, M.F. Nazar, A. Mahmood, Quantum chemical designing of efficient TC4-based sensitizers by modification of auxiliary donor and π-spacer. Bull. Chem.

Soc. Jpn **86**, 1272–1281 (2013). https://doi.org/10.1246/bcsj.20130146
18. M.R.S.A. Janjua, Z.M. Su, W. Guan, C.G. Liu, L.K. Yan, P. Song, G. Maheen, Tuning second-order non-linear (NLO) optical response of organoimido-substituted hexamolybdates through halogens: quantum design of novel organic-inorganic hybrid NLO materials. Aust. J. Chem. **63**, 836 (2010). https://doi.org/10.1071/CH10094
19. M.R.S.A. Janjua, W. Guan, L. Yan, Z. Su, A. Karim, J. Akbar, Quantum chemical design for enhanced second-order NLO response of terpyridine-substituted hexamolybdates. Eur. J. Inorg. Chem. **2010**, 3466–3472 (2010). https://doi.org/10.1002/ejic.201000428
20. M.R.S.A. Janjua, S. Jamil, A. Mahmood, A. Zafar, M. Haroon, H.N. Bhatti, Solvent-dependent non-linear optical properties of 5,5′-disubstituted-2,2′-bipyridine complexes of ruthenium(II): a quantum chemical perspective. Aust. J. Chem. **68**, 1502–1507 (2015). https://doi.org/10.1071/CH14736
21. M.R.S.A. Janjua, A. Mahmood, F. Ahmad, Solvent effects on nonlinear optical response of certain tetramminerutheniumII) complexes of modified 1,10-phenanthrolines. Can. J. Chem. **91**, 1303–1309 (2013). https://doi.org/10.1139/cjc-2013-0377
22. M.R.S.A. Janjua, Quantum chemical design of d–π–a-type donor materials for highly efficient, photostable, and vacuum-processed organic solar cells. Energy Technol. **9**, 1–12 (2021). https://doi.org/10.1002/ente.202100489
23. M.R.S.A. Janjua, Theoretical framework for encapsulation of inorganic $B_{12}N_{12}$ nanoclusters with alkaline earth metals for efficient hydrogen adsorption: a step forward toward hydrogen storage materials. Inorg. Chem. **60**, 2816–2828 (2021). https://doi.org/10.1021/acs.inorgchem.0c03730
24. M.R.S.A. Janjua, W. Guan, L. Yan, Z.M. Su, M. Ali, I.H. Bukhari, Prediction of robustly large molecular second-order nonlinear optical properties of terpyridine-substituted hexamolybdates: structural modelling towards a rational entry to NLO materials. J. Mol. Graph. Model. **28**, 735–745 (2010). https://doi.org/10.1016/j.jmgm.2010.01.011
25. M.R.S.A. Janjua, A. Irfan, M. Hussien, M. Ali, M. Saqib, M. Sulaman, Machine-learning analysis of small-molecule donors for fullerene based organic solar cells. Energy Technol. **10**, 2200019 (2022). https://doi.org/10.1002/ente.202200019
26. M.R.S.A. Janjua, Nonlinear optical response of a series of small molecules: quantum modification of π-spacer and acceptor. J. Iran. Chem. Soc. **14**, 2041–2054 (2017). https://doi.org/10.1007/s13738-017-1141-x
27. S.R. Maidur, J.R. Jahagirdar, P.S. Patil, T.S. Chia, C.K. Quah, Structural characterizations, Hirshfeld surface analyses, and third-order nonlinear optical properties of two novel chalcone derivatives. Opt. Mater. **75**, 580–594 (2018). https://doi.org/10.1016/j.optmat.2017.11.008
28. M.K.M. Ali, A. Elzupir, M.A. Ibrahem, I.I. Suliman, A. Modwi, H. Idriss, K.H. Ibnaouf, Characterization of optical and morphological properties of chalcone thin films for optoelectronics applications. Optik **145**, 529–533 (2017). https://doi.org/10.1016/j.ijleo.2017.08.044
29. L.F. Sciuti, C.H.D. Dos Santos, L.H.Z. Cocca, A.G. Pelosi, R.G.M. da Costa, J. Limberger, C.R. Mendonça, L. De Boni, Studying the first order hyperpolarizability spectra in chalcone-based derivatives and the relation with one- and two-photon absorption transitions. J. Chem. Phys. **159**, 244311 (2023). https://doi.org/10.1063/5.0166036
30. A. Aditya Prasad, K. Muthu, V. Meenatchi, M. Rajasekar, R. Agilandeshwari, K. Meena, J. Vijila Manonmoni, S.P. Meenakshisundaram, Optical, vibrational, NBO, first-order molecular hyperpolarizability and Hirshfeld surface analysis of a nonlinear optical chalcone. Spectrochim. Acta Part A Mol. Biomol. Spectrosc. **140**, 311–327 (2015). https://doi.org/10.1016/j.saa.2014.12.011
31. S. Muhammad, A.G. Al-Sehemi, A. Irfan, A.R. Chaudhry, H. Gharni, S. AlFaify, M. Shkir, A.M. Asiri, The impact of position and number of methoxy group(s) to tune the nonlinear optical properties of chalcone derivatives: a dual substitution strategy. J. Mol. Model. **22**, 73 (2016). https://doi.org/10.1007/s00894-016-2946-8
32. M. Haroon, M.R.S.A. Janjua, High-throughput designing and investigation of D-A−π–A-type donor materials for potential application in greenhouse-integrated solar cells. Energy Fuels **35**, 12461–12472 (2021). https://doi.org/10.1021/acs.energyfuels.1c01726
33. M.Y. Mehboob, R. Hussain, M. Adnan, Saira, U. Farwa, Z. Irshad, M.R.S.A. Janjua, Theoretical modelling of novel indandione-based donor molecules for organic solar cell applications. J. Phys. Chem. Solids **162**, 110508 (2022). https://doi.org/10.1016/j.jpcs.2021.110508
34. M.R.S.A. Janjua, How does bridging core modification alter the photovoltaic characteristics of triphenylamine-based hole transport materials? Theoretical understanding and prediction. Chem. Eur. J. **27**, 4197–4210 (2021). https://doi.org/10.1002/chem.202004299
35. M.R.S.A. Janjua, All-small-molecule organic solar cells with high fill factor and enhanced open-circuit voltage with 18.25 % PCE: physical insights from quantum chemical calculations. Spectrochim. Acta. A Mol. Biomol. Spectrosc. **279**, 121487 (2022). https://doi.org/10.1016/j.saa.2022.121487
36. M.J. Frisch, G.W. Trucks, H.B. Schlegel, G.E. Scuseria, M.A. Robb, J.R. Cheeseman, G. Scalmani, V. Barone, B. Mennucci, G.A. Petersson, H. Nakatsuji, M. Caricato, X. Li, H.P. Hratchian, A.F. Izmaylov, J. Bloino, G. Zheng, J.L. Sonnenberg, M. Hada, M. Ehara, K. Toyota, R. Fukuda, J. Hasegawa, M. Ishida, T. Nakajima, Y. Honda, O. Kitao, H. Nakai, T. Vreven, J.A. Montgomery Jr., J.E. Peralta, F. Ogliaro, M. Bearpark, J.J. Heyd, E. Brothers, K.N. Kudin, V.N. Staroverov, R. Kobayashi, J.Normand, K. Raghavachari, A. Rendell, J.C. Burant, S.S. Iyengar, J. Tomasi, M. Cossi, N. Rega, J.M. Millam, M. Klene, J.E. Knox, J.B. Cross, V. Bakken, C. Adamo, J. Jaramillo, R. Gomperts, R.E. Stratmann, O. Yazyev, A.J. Austin, R. Cammi, C.Pomelli, J.W. Ochterski, R.L. Martin, K., Vol. Morokuma, V.G. Zakrzewski, G.A. Voth, P. Salvador, J.J. Dannenberg, S. Dapprich, A.D. Daniels, J.B. Foresman, J.V. Ortiz, J. Cioslowski, D.J. Fox, Gaussian 09, Gaussian, Inc., Wallingford CT (2009).
37. F. Hammami, N. Issaoui, S. Nasr, Investigation of hydrogen bonded structure of urea-water mixtures through Infra-red spectroscopy and non-covalent interaction (NCI) theoretical approach. Comput. Theor. Chem. **1199**, 113218 (2021). https://doi.org/10.1016/j.comptc.2021.113218
38. M. Medimagh, C. Ben Mleh, N. Issaoui, A.S. Kazachenko, T. Roisnel, O.M. Al-Dossary, H. Marouani, L.G. Bousiakoug, DFT and molecular docking study of the effect of a green solvent (water and DMSO) on the structure, MEP, and FMOs of the 1-ethylpiperazine-1,4-diium bis(hydrogenoxalate) compound. J. Mol. Liq. **369**, 120851 (2023). https://doi.org/10.1016/j.molliq.2022.120851
39. R. Dennington, T. Keith, J.M. Millam, *GaussView version 5* (SemichemInc., Shawnee Mission, Fairway) (2009)
40. L.S. Kassel, The limiting high temperature rotational partition function of nonrigid molecules. I. General theory. II. CH_4, C_2H_6, C_3H_8, $CH(CH_3)_3$, $C(CH_3)_4$ and $CH_3(CH_2)_2CH_3$. III. Benzene and its eleven methyl derivatives. J. Chem. Phys. **4**, 276–282 (1936). https://doi.org/10.1063/1.1749835
41. P.J. Stephens, F.J. Devlin, C.F. Chabalowski, M.J. Frisch, Ab initio calculation of vibrational absorption and circular dichroism

spectra using density functional force fields. J. Phys. Chem. **98**, 11623–11627 (1994). https://doi.org/10.1021/j100096a001
42. C. Adamo, M. Cossi, G. Scalmani, V. Barone, Accurate static polarizabilities by density functional theory: assessment of the PBE0 model. Chem. Phys. Lett. **307**, 265–271 (1999). https://doi.org/10.1016/S0009-2614(99)00515-1
43. T. Yanai, D.P. Tew, N.C. Handy, A new hybrid exchange-correlation functional using the Coulomb-attenuating method (CAM-B3LYP). Chem. Phys. Lett. **393**, 51–57 (2004). https://doi.org/10.1016/j.cplett.2004.06.011
44. J.-D. Chai, M. Head-Gordon, Systematic optimization of long-range corrected hybrid density functionals. J. Chem. Phys. **128**, 084106 (2008). https://doi.org/10.1063/1.2834918
45. Y. Zhao, D.G. Truhlar, Density functional for spectroscopy: no long-range self-interaction error, good performance for Rydberg and charge-transfer states, and better performance on average than B3LYP for ground states. J. Phys. Chem. A **110**, 13126–13130 (2006). https://doi.org/10.1021/jp066479k
46. T. Lu, F. Chen, Multiwfn: a multifunctional wavefunction analyzer. J. Comput. Chem. **33**, 580–592 (2012). https://doi.org/10.1002/jcc.22885
47. D. Hadji, B. Champagne, First principles investigation of the polarizability and first hyperpolarizability of anhydride derivatives. Chem. Afr. **2**, 443–453 (2019). https://doi.org/10.1007/s42250-019-00060-3
48. D. Hadji, A. Rahmouni, Molecular structure, linear and nonlinear optical properties of some cyclic phosphazenes: a theoretical investigation. J. Mol. Struct. **1106**, 343–351 (2016). https://doi.org/10.1016/j.molstruc.2015.10.033
49. D.R. Kanis, M.A. Ratner, T.J. Marks, Design and construction of molecular assemblies with large second-order optical nonlinearities. Quantum chemical aspects. Chem. Rev. **94**, 195–242 (1994). https://doi.org/10.1021/cr00025a007
50. R. Bersohn, P.A.O. Yoh-Han, H.L. Frisch, Double-quantum light scattering by molecules. J. Chem. Phys. **45**, 3184–3198 (1966). https://doi.org/10.1063/1.1728092
51. Q. Zhao, J. Qu, F. He, Chlorination: an effective strategy for high-performance organic solar cells. Adv. Sci. **7**, 1–25 (2020). https://doi.org/10.1002/advs.202000509
52. A.S. Salim, A.H. Bedair, Comparative DFT computational studies with experimental investigations for novel synthesized fluorescent pyrazoline derivatives. J. Fluoresc. **28**, 913–931 (2018). https://doi.org/10.1007/s10895-018-2254-z
53. H. Zhang, H. Yao, J. Hou, J. Zhu, J. Zhang, W. Li, R. Yu, B. Gao, S. Zhang, J. Hou, Over 14% efficiency in organic solar cells enabled by chlorinated nonfullerene small-molecule acceptors. Adv. Mater. **30**, 1–7 (2018). https://doi.org/10.1002/adma.201800613
54. D. Hadji, T. Bensafi, Deeper insights on the nonlinear optical properties of *o*-acylated pyrazoles. J. Electron. Mater. **53**, 1868–1883 (2024). https://doi.org/10.1007/s11664-024-10954-9
55. W. Kumler, G. Fohlen, Additions and corrections: the dipole moment and structure of urea and thiourea. J. Am. Chem. Soc. **64**, 3071–3071 (1942). https://doi.org/10.1021/ja01264a626
56. T. Andrade-Filho, T. Silva, E. Belo, A. Raiol, R.V.S. de Oliveira, P.S.B. Marinho, H.R. Bitencourt, A.M.R. Marinho, A.R. da Cunha, R. Gester, Insights and modelling on the nonlinear optical response, reactivity, and structure of chalcones and dihydrochalcones. J. Mol. Struct. **1246**, 131182 (2021). https://doi.org/10.1016/j.molstruc.2021.131182
57. S. Muhammad, A.G. Al-Sehemi, Z. Su, H. Xu, A. Irfan, A.R. Chaudhry, First principles study for the key electronic, optical and nonlinear optical properties of novel donor-acceptor chalcones. J. Mol. Graph. Model. **72**, 58–69 (2017). https://doi.org/10.1016/j.jmgm.2016.12.009
58. N.E.H. Nourai, F. Sebih, D. Hadji, F.Z. Allal, S. Dib, N. Kambouche, V. Rolland, S. Bellahouel-Benzine, Nonlinear optical and antimicrobial activity of N-acyl glycine derivatives. J. Mol. Liq. **398**, 124260 (2024). https://doi.org/10.1016/j.molliq.2024.124260
59. D. Hadji, H. Brahim, Structural, optical and nonlinear optical properties and TD-DFT analysis of heteroleptic bis-cyclometalated iridium(III) complex containing 2-phenylpyridine and picolinate ligands. Theor. Chem. Acc. **137**, 180 (2018). https://doi.org/10.1007/s00214-018-2396-8
60. M. Boukabene, H. Brahim, D. Hadji, A. Guendouzi, Theoretical study of geometric, optical, nonlinear optical, UV–Vis spectra and phosphorescence properties of iridium(III) complexes based on 5-nitro-2-(2′,4′-difluorophenyl)pyridyl. Theor. Chem. Acc. **139**, 47 (2020). https://doi.org/10.1007/s00214-020-2560-9
61. A. Benmohammed, D. Hadji, A. Guendouzi, Y. Mouchaal, A. Djafri, A. Khelil, Synthesis, characterization, linear and NLO properties of novel N-(2,4-dinitrobenzylidene)-3-chlorobenzenamine Schiff base: combined experimental and DFT calculations. J. Electron. Mater. **50**, 5282–5293 (2021). https://doi.org/10.1007/s11664-021-09046-9
62. D. Hadji, A. Benmohammed, Y. Mouchaal, A. Djafri, Synthesis and characterization of novel thiosemicarbazide for nonlinear optical applications: combined experimental and theoretical study. Rev. Roum. Chim. **68**, 463–471 (2023). https://doi.org/10.33224/rrch.2023.68.9.07
63. T. Bensafi, D. Hadji, A. Yahiaoui, K. Argoub, A. Hachemaoui, A. Kenane, B. Baroudi, K. Toubal, A. Djafri, A.M. Benkouider, Synthesis, characterization and DFT calculations of linear and NLO properties of novel (Z)-5-benzylidene-3-N(4-methylphenyl)-2-thioxothiazolidin-4-one. J. Sulfur Chem. **42**, 645–663 (2021). https://doi.org/10.1080/1741599320211951729
64. B. Baroudi, K. Argoub, D. Hadji, A.M. Benkouider, K. Toubal, A. Yahiaoui, A. Djafri, Synthesis and DFT calculations of linear and nonlinear optical responses of novel 2-thioxo-3-N,(4-methylphenyl) thiazolidine-4 one. J. Sulfur Chem. **41**, 310–325 (2020). https://doi.org/10.1080/17415993.2020.1736073
65. D. Hadji, K. Bousmaha, M. Boumediene, NLO azo compounds with sulfonamide groups: a theoretical investigation. J. Indian Chem. Soc. **100**, 101062 (2023). https://doi.org/10.1016/j.jics.2023.101062
66. A. Kenane, D. Hadji, K. Argoub, A. Yahiaoui, A. Hachemaoui, K. Toubal, A.M. Benkouider, O. Rasoga, A. Stanculescu, A. Galca, Efficient NLO materials based on poly(ortho-anisidine) and polyaniline: a quantum chemical study. J. Electron. Mater. **52**, 530–539 (2023). https://doi.org/10.1007/s11664-022-10022-0
67. Y. Bekki, D. Hadji, A. Guendouzi, B. Houari, M. Elkeurti, Linear and nonlinear optical properties of anhydride derivatives: a theoretical investigation. Chem. Data Collect. **37**, 100809 (2022). https://doi.org/10.1016/j.cdc.2021.100809
68. D. Hadji, A. Rahmouni, Theoretical study of nonlinear optical properties of some azoic dyes. Mediterr. J. Chem. **4**, 185–192 (2015). https://doi.org/10.13171/mjc.4.4.2015.15.07.22.50/hadji
69. D. Hadji, B. Haddad, S.A. Brandán, S.K. Panja, A. Paolone, M. Drai, D. Villemin, S. Bresson, M. Rahmouni, Synthesis, NMR, Raman, thermal and nonlinear optical properties of dicationic ionic liquids from experimental and theoretical studies. J. Mol. Struct. **1220**, 128713 (2020). https://doi.org/10.1016/j.molstruc.2020.128713
70. F.Y. Cherif, D. Hadji, N. Benhalima, Molecular structure, linear, and nonlinear optical properties of piperazine-1,4-diium bis 2,4,6-trinitrophenolate: a theoretical investigation. Phys. Chem. Res. **11**, 33–48 (2023). https://doi.org/10.22036/pcr.2022.330752.2035

71. R. Gheribi, D. Hadji, R. Ghallab, M. Medjani, M. Benslimane, C. Trifa, G. Dénès, H. Merazig, Synthesis, spectroscopic characterization, crystal structure, Hirshfeld surface analysis, linear and NLO properties of new hybrid compound based on tin fluoride oxalate and organic amine molecule $(C_{12}N_2H_9)_2[SnF_2(C_2O_4)_2]_2H_2O$. J. Mol. Struct. **1248**, 131392 (2022). https://doi.org/10.1016/j.molstruc.2021.131392
72. Z. Liu, Z. Tian, T. Lu, S. Hua, Theoretical framework of 1,3-thiazolium-5-thiolates mesoionic compounds: exploring the nature of photophysical property and molecular nonlinearity. J. Phys. Chem. A **124**, 5563–5569 (2020). https://doi.org/10.1021/acs.jpca.0c03166
73. M. Haroon, M.R.S.A. Janjua, Exploring the effect of end-capped modifications of carbazole-based fullerene-free acceptor molecules for high-performance indoor organic solar cell applications. J. Comput. Electron. **21**, 40–51 (2022). https://doi.org/10.1007/s10825-021-01838-w
74. R. Mahmood, M.R.S.A. Janjua, S. Jamil, DFT molecular simulation for design and effect of core bridging acceptors (BA) on NLO response: first theoretical framework to enhance nonlinearity through BA. J. Clust. Sci. **28**, 3175–3183 (2017). https://doi.org/10.1007/s10876-017-1287-9
75. M.R.S.A. Janjua, First theoretical framework of di-substituted donor moieties of triphenylamine and carbazole for NLO properties: quantum paradigms of interactive molecular computation. Mol. Simul. **43**, 1539–1545 (2017). https://doi.org/10.1080/08927022.2017.1332413
76. S. Gatfaoui, N. Issaoui, T. Roisnel, H. Marouani, Synthesis, experimental and computational study of a non-centrosymmetric material 3-methylbenzylammonium trioxonitrate. J. Mol. Struct. **1225**, 129132 (2021). https://doi.org/10.1016/j.molstruc.2020.129132
77. C. Daghar, N. Issaoui, T. Roisnel, V. Dorcet, H. Marouani, Empirical and computational studies on newly synthesis cyclohexylammonium perchlorate. J. Mol. Struct. **1230**, 129820 (2021). https://doi.org/10.1016/j.molstruc.2020.129820
78. N. Mhadhbi, N. Issaoui, W.S. Hamadou, J.M. Alam, A.S. Elhadi, M. Adnan, H. Naïli, R. Badraoui, Physico-chemical properties, pharmacokinetics, molecular docking and in-vitro pharmacological study of a cobalt (II) complex based on 2-aminopyridine. ChemistrySelect **7**, e202103592 (2022). https://doi.org/10.1002/slct.202103592
79. A. Merouane, A. Mostefai, D. Hadji, A. Rahmouni, M. Bouchekara, A. Ramdani, S. Taleb, Theoretical insights into the static chemical reactivity and NLO properties of some conjugated carbonyl compounds: case of 5-aminopenta-2,4-dienal derivatives. Monatshefte Für Chemie Chem. Mon. **151**, 1095–1109 (2020). https://doi.org/10.1007/s00706-020-02653-y
80. M. Basharat, D. Hadji, Theoretical insights into the nonlinear optical properties of cyclotriphosphazene $(P_3N_3Cl_6)$, tris(4-hydroxyphenyl) ethane and their various inorganic–organic hybrid derivatives. J. Mater. Sci. **57**, 6971–6987 (2022). https://doi.org/10.1007/s10853-022-07088-w
81. D. Hadji, A. Rahmouni, D. Hammoutène, O. Zekri, First theoretical study of linear and nonlinear optical properties of diphenyl ferrocenyl butene derivatives. J. Mol. Liq. **286**, 110939 (2019). https://doi.org/10.1016/j.molliq.2019.110939
82. D. Hadji, Phosphates branching effect on the structure, linear and NLO properties of linear phosphazenes. Mater. Chem. Phys. **262**, 124280 (2021). https://doi.org/10.1016/j.matchemphys.2021.124280
83. Y. Xue, J. Mou, Y. Liu, X. Gong, Y. Yang, L. An, An ab initio simulation of the UV/Visible spectra of substituted chalcones. Open Chem. **8**, 928–936 (2010). https://doi.org/10.2478/s11532-010-0058-3
84. V.S. Naik, P.S. Patil, N.B. Gummagol, Q.A. Wong, C.K. Quah, H.S. Jayanna, Crystal structure, linear and nonlinear optical properties of three thiophenyl chalcone derivatives: a combined experimental and computational study. Opt. Mater. **110**, 110462 (2020). https://doi.org/10.1016/j.optmat.2020.110462
85. M. Basharat, Y. Abbas, D. Hadji, Z. Ali, S. Zhang, H. Ma, Z. Wu, W. Liu, Amorphous covalent inorganic–organic hybrid frameworks (CIOFs) with an aggregation induced selective response to UV–Visible light and their DFT studies. J. Mater. Chem. C **8**, 13612–13620 (2020). https://doi.org/10.1039/D0TC01535K
86. G.W. Ejuh, C. Fonkem, Y. Tadjouteu Assatse, R.A. Yossa Kamsi, T. Nya, L.P. Ndukum, J.M.B. Ndjaka, Study of the structural, chemical descriptors and optoelectronic properties of the drugs hydroxychloroquine and Azithromycin. Heliyon **6**, e04647 (2020). https://doi.org/10.1016/j.heliyon.2020.e04647
87. T. Bensafi, D. Hadji, Quantum chemical exploration of linear and nonlinear optical characteristics in *C*-acylated pyrazoles. *Opt. Quantum Electron.* (2024) Accepted paper
88. M. Fathimunnisa, H. Manikandan, S. Selvanayagam, Synthesis of novel (2E)-1-[4-(2,4-difluorophenyl)phenyl]3-arylprop-2-en-1-ones: investigation on spectral, antibacterial, molecular docking and theoretical studies. J. Mol. Struct. **1099**, 407–418 (2015). https://doi.org/10.1016/j.molstruc.2015.06.078
89. O. Noureddine, N. Issaoui, M. Medimagh, O. Al-Dossary, H. Marouani, Quantum chemical studies on molecular structure, AIM, ELF, RDG and antiviral activities of hybrid hydroxychloroquine in the treatment of COVID-19: molecular docking and DFT calculations. J. King Saud Univ. Sci. **33**, 101334 (2021). https://doi.org/10.1016/j.jksus.2020.101334
90. O. Noureddine, S. Gatfaoui, S.A. Brandan, A. Sagaama, H. Marouani, N. Issaoui, Experimental and DFT studies on the molecular structure, spectroscopic properties, and molecular docking of 4-phenylpiperazine-1-ium dihydrogen phosphate. J. Mol. Struct. **1207**, 127762 (2020). https://doi.org/10.1016/j.molstruc.2020.127762
91. N. Issaoui, H. Ghalla, F. Bardak, M. Karabacak, N. Aouled Dlala, H.T. Flakus, B. Oujia, Combined experimental and theoretical studies on the molecular structures, spectroscopy, and inhibitor activity of 3-(2-thienyl)acrylic acid through AIM, NBO, FT-IR, FT-Raman, UV and HOMO-LUMO analyses, and molecular docking. J. Mol. Struct. **1130**, 659–668 (2017). https://doi.org/10.1016/j.molstruc.2016.11.019
92. H. Ghalla, N. Issaoui, F. Bardak, A. Atac, Intermolecular interactions and molecular docking investigations on 4-methoxybenzaldehyde. Comput. Mater. Sci. **149**, 291–300 (2018). https://doi.org/10.1016/j.commatsci.2018.03.042
93. A. Sagaama, S.A. Brandan, T. BenIssa, N. Issaoui, Searching potential antiviral candidates for the treatment of the 2019 novel coronavirus based on DFT calculations and molecular docking. Heliyon **6**, e04640 (2020). https://doi.org/10.1016/j.heliyon.2020.e04640
94. O. Noureddine, S. Gatfaoui, S.A. Brandán, H. Marouani, N. Issaoui, Structural, docking and spectroscopic studies of a new piperazine derivative, 1-Phenylpiperazine-1,4-diium bis(hydrogen sulfate). J. Mol. Struct. **1202**, 127351 (2020). https://doi.org/10.1016/j.molstruc.2019.127351
95. R.G. Pearson, Hard and soft acids and bases, HSAB, part 1: fundamental principles. J. Chem. Educ. **45**, 581 (1968). https://doi.org/10.1021/ed045p581
96. R.G. Pearson, Absolute electronegativity and hardness: applications to organic chemistry. J. Org. Chem. **54**, 1423–1430 (1989). https://doi.org/10.1021/jo00267a034
97. R.G. Pearson, Hard and soft acids and bases. J. Am. Chem. Soc. **85**, 3533–3539 (1963). https://doi.org/10.1021/ja00905a001

98. M. Samsonowicz, E. Regulska, R. Świsłocka, A. Butarewicz, Molecular structure and microbiological activity of alkali metal 3,4-dihydroxyphenylacetates. J. Saudi Chem. Soc. **22**, 896–907 (2018). https://doi.org/10.1016/j.jscs.2018.01.009
99. T.A. Yousef, G.M. Abu El-Reash, R.M. El Morshedy, Structural, spectral analysis and DNA studies of heterocyclic thiosemicarbazone ligand and its Cr(III), Fe(III), Co(II) Hg(II), and U(VI) complexes. J. Mol. Struct. **1045**, 145–159 (2013). https://doi.org/10.1016/j.molstruc.2013.03.060
100. G. Venkatesh, S. Haseena, J.S. Al-Otaibi, Y.S. Mary, P. Vennila, Y. Shyma Mary, S.A.K. Azad, Observations into the reactivity, docking, DFT, and MD simulations of fludarabine and clofarabine in various solvents. J. Mol. Liq. **383**, 122076 (2023). https://doi.org/10.1016/j.molliq.2023.122076
101. M. Muthukkumar, T. Bhuvaneswari, G. Venkatesh, C. Kamal, P. Vennila, S. Armaković, S.J. Armaković, Y. Sheena Mary, C. Yohannan Panicker, Synthesis, characterization and computational studies of semicarbazide derivative. J. Mol. Liq. **272**, 481–495 (2018). https://doi.org/10.1016/j.molliq.2018.09.123
102. P.K. Chattaraj, U. Sarkar, D.R. Roy, Electrophilicity index. Chem. Rev. **106**, 2065–2091 (2006). https://doi.org/10.1021/cr040109f
103. R.G. Parr, L.V. Szentpály, S. Liu, Electrophilicity index. J. Am. Chem. Soc. **121**, 1922–1924 (1999). https://doi.org/10.1021/ja983494x
104. A. Nataraj, V. Balachandran, T. Karthick, Molecular orbital studies (hardness, chemical potential, electrophilicity, and first electron excitation), vibrational investigation and theoretical NBO analysis of 2-hydroxy-5-bromobenzaldehyde by density functional method. J. Mol. Struct. **1031**, 221–233 (2013). https://doi.org/10.1016/j.molstruc.2012.09.047
105. P. Pérez, L.R. Domingo, A. Aizman, R. Contreras, Chapter 9 the electrophilicity index in organic chemistry, in: *Theoretical and Computational Chemistry*, vol. 19, pp. 139–201 (2007). https://doi.org/10.1016/S1380-7323(07)80010-0